Joint Transceiver Optimization for Wireless Information and Energy Transfer in Nonregenerative MIMO Relay Systems

Bin Li, *Senior Member, IEEE*, and Yue Rong, *Senior Member, IEEE*

***Abstract*—In this paper, a two-hop nonregenerative multiple-input multiple-output relay system is investigated, where the relay node relies on harvesting the radio frequency energy transferred from the source node to forward information from source to destination. We consider the time switching (TS) protocol between wireless information and energy transfer. In particular, we propose a more general energy consumption constraint at the source node during the information and energy transfer, which includes the constant power constraints used in existing works as special cases. We study the joint optimization of the source precoding matrices, the relay amplifying matrix, and the TS factor to maximize the source–destination mutual information (MI). The optimal structure of the source and relay matrices is derived, which reduces the original transceiver optimization problem to a simpler power allocation problem. We propose a primal decomposition based algorithm and an upper bound based approach to efficiently solve the power allocation problem. The first algorithm achieves the global optimum, whereas the latter one has a lower computational complexity. Numerical simulations show that both proposed algorithms yield much higher system MI and better rate-energy tradeoff than existing approaches.**

***Index Terms*—Simultaneous wireless information and energy transfer (SWIET), energy harvesting, time switching receiver, MIMO relay, nonregenerative relay.**

I. Introduction

A. Background

THERE have been many successful applications of wireless sensor networks (WSNs) in intelligent transportation and environmental monitoring [1]. However, WSNs are energy-constrained networks which are normally powered by batteries that have a limited life time. Although replacing batteries is an option that can prolong the life time of a WSN, a high cost is usually associated. Moreover, in many cases, replacing batteries cannot be easily carried out due to physical or economic constraints. For example, sometimes the sensors may be embedded in building structures or even inside human bodies [2].

Therefore, energy harvesting (EH) is attractive for WSNs, where energy is harvested from the external environment. Conventional EH techniques, which mainly rely on natural resources (such as solar and wind), have their limitations in that these energy is difficult to be controlled. Hence, these techniques are not easy to be implemented in real world applications.

To overcome the limitations of conventional EH techniques, a new technology called simultaneous wireless information and energy transfer (SWIET) has been proposed [3]. With SWIET, radio frequency (RF) signals are used not only for delivering information but also for transferring energy, which provides great convenience to WSNs and mobile users [4]. Compared with conventional EH techniques relying on nature resources, SWIET is a more promising and reliable alternative.

B. Literature Review

An ideal receiver capable of performing information decoding (ID) and EH simultaneously has been proposed in [3]. The tradeoff between the achievable information rate and the harvested energy is also characterized by a capacity-energy function in [3]. However, there are two challenges from practical considerations [4]. Firstly, in practice, the circuits for harvesting energy cannot decode the carried information. To coordinate wireless information transfer (WIT) and wireless energy transfer (WET) at the receiver, a time switching (TS) protocol and a power splitting (PS) protocol have been proposed in [5]. Secondly, since WIT and WET operate with different sensitivity (-10 dBm for energy receivers and -60 dBm for information receivers), the architecture of traditional ID receiver may not be optimal for SWIET. To solve this problem, a separated architecture receiver and an integrated architecture receive have been developed in [4] for a more general protocol called dynamic power splitting which includes the TS protocol and the PS protocol as special cases. Waveform design for wireless power transfer has been studied in [6] and [7].

It is well-known that multiple-input multiple-output (MIMO) technique can improve the system energy and spectral efficiencies [8]–[10]. By equipping multiple antennas at the data fusion center of WSNs, RF energy can be focused on sensors so that they can be charged more efficiently compared with using a single antenna. Hence, the life time of energy constrained WSNs is prolonged. There are some recent works on applying MIMO

Manuscript received November 9, 2017; revised February 16, 2018 and April 23, 2018; accepted June 8, 2018. Date of publication June 12, 2018; date of current version September 17, 2018. This work was supported in part by the National Natural Science Foundation of China under Grant 61701124, in part by the Fundamental Research Funds for the Central Universities (China), and in part by the Australian Research Council's Discovery Projects funding scheme under Grant DP140102131. This paper was presented in part at the Twenty Third Asia-Pacific Conference on Communications, Perth, WA, Australia, December 2017. The review of this paper was coordinated by Dr. H. Zhu. *(Corresponding author: Yue Rong.)*

B. Li is with the School of Electrical Engineering and Information, Sichuan University, Chengdu 610065, China (e-mail: bin.li@scu.edu.cn).

Y. Rong is with the Department of Electrical and Computer Engineering, Curtin University, Perth WA 6845, Australia (e-mail: y.rong@curtin.edu.au).

Color versions of one or more of the figures in this paper are available online at http://ieeexplore.ieee.org.

Digital Object Identifier 10.1109/TVT.2018.2846556

to SWIET. In [5], a MIMO broadcast channel with a separated architecture ID and EH receiver has been investigated, where the energy-rate regions have been derived for the TS protocol and the PS protocol. In [11], a multiple-input single-output (MISO) downlink system has been considered with SWIET, where the total transmission power is minimized by jointly optimizing the transmit beamforming vector and the PS ratio under a given signal-to-interference-plus-noise ratio (SINR).

Relay technology has been widely used to increase the coverage of wireless communications [13], [14]. Under the SWIET framework, a relay node is able to harvest RF energy and receive information from the source node and then forwards the received information to the destination node using the harvested energy. The application of relays in SWIET has been addressed by some recent works [15]–[22]. In [15], TS and PS based relay protocols have been proposed for a non-regenerative relay network. A wireless cooperative network has been considered in [16] where multiple source-destination pairs communicate with each other via an EH relay node. The distribution of the harvested energy among multiple users and its impact on the system performance have been studied in [16]. SWIET with randomly located decode-and-forward relays has been studied in [17], and it has been shown that the use of EH relays can achieve the same diversity gain as conventional self-powered relays. In [18], a distributed PS framework based on game theory has been developed for SWIET in interference relay channels. SWIET in an orthogonal frequency-division multiplexing relay system has been studied in [19]. Wireless information and power transfer with full duplex relaying has been investigated recently in [20]–[22].

The application of SWIET in MIMO relay systems has been studied in [1], [2], [23]–[29]. In [1], performance trade-offs of several receiver architectures have been discussed by applying SWIET in MIMO relay systems. Future research challenges in this area have also been outlined in [1]. A TS protocol and a PS protocol have been developed in [2] for a non-regenerative MIMO relay system, where the achievable rate is maximized for each protocol by jointly optimizing the source and relay precoding matrices. In [23] and [24], a non-regenerative orthogonal space-time block code (OSTBC) based MIMO relay system with a multi-antenna EH receiver has been investigated, where the source and relay precoding matrices are jointly optimized to achieve various tradeoffs between the energy transfer capability and the information rate. SWIET for wireless cooperative networks with the PS protocol has been studied in [25], where the optimal PS ratio and power allocation are obtained. SWIET in massive MIMO relay networks has been investigated in [26]. Joint wireless information and power transfer in amplify-and-forward (AF) MIMO relay systems with wireless powered relay node has been considered in [27]–[29].

C. Contributions

In this paper, we consider a two-hop non-regenerative MIMO relay system, where an EH receiver is equipped at the relay node to facilitate the information and energy transfer. One example of practical applications of the system and algorithms proposed in this paper is a heterogeneous network consisting of devices with different capabilities, where inactive devices with MIMO capabilities can be exploited as relays to assist the active users in the network [1]. Moreover, through harvesting the radio frequency energy transferred from the source node, the relay node does not need to spend its own energy to forward information from source to destination. This helps to provide motivation for a selfish node to participate in the relay scheme. We adopt the TS protocol during the source phase, where the source node transfers energy and information signals to the relay node during the first and second time intervals, respectively. Then, during the relay phase, the relay node uses the harvested energy to forward the received information to the destination node.

In [2], a constant power is assumed at the source node for both energy transferring and information transmission. Here, we propose an energy consumption constraint at the source node during the information and energy transfer. For the fairness of comparison, our energy consumption constraint is formulated under the same nominal power as that in [2]. However, compared with the formulation in [2], the source transmission power for energy and information transferring might be different. Therefore, the proposed energy constraint is more general and includes the constant power constraints in [2] as special cases, and hence, a better performance can be expected. Note that compared with the constant power constraint, the energy consumption constraint greatly increases the technical difficulty of solving the optimization problem.

We study the joint optimization of the source precoding matrices, the relay amplifying matrix, and the TS factor to maximize the source-destination mutual information (MI), subjecting to the harvested energy constraint at the relay node and the proposed source energy constraint at the source node. Moreover, the circuit power consumption at the relay node is considered in the transceiver optimization. The optimal structure of the source and relay matrices is derived, which reduces the matrix variables to vector power allocation variables. Based on the observation that the system MI is a unimodal function of the TS factor, we develop a two-loop method to jointly optimize the TS factor and the power allocation vectors.

In particular, we show that the optimal TS factor can be efficiently found by a golden section search [30]. In each step of the search for the optimal TS factor, the power allocation vectors are optimized through solving a power allocation problem in a two-hop non-regenerative MIMO relay system with sum power constraint across the source and relay nodes. We propose a primal decomposition technique [31] to solve this power allocation problem. In particular, we derive the closed-form analytical solution to each of the decomposed subproblems. Moreover, as the traditional water-filling algorithm does not work for the master problem, we develop a novel algorithm by exploring the structure of the master problem. The optimality of the primal decomposition based algorithm is proven rigorously. To the best of our knowledge, the globally optimal solution to such power allocation problem is obtained for the first time in this paper.

To reduce the computational complexity of the primal decomposition based algorithm, we propose a second algorithm by exploiting a tight upper bound of the objective function. We show that the upper bound based problem has a closed-form solution and a similar performance as that of the primal decomposition based approach. Interestingly, we prove that at a large power level, the upper bound based system MI is a strictly convex function of the TS factor.

The contributions of this paper are summarized as follows: (1) For the first time, a more general energy constraint at the source node is proposed compared with that in [2]; (2) The optimal structure of the source and relay precoding matrices is proven for the new problem; (3) For the first time, the global optimum solution is obtained for the power allocation problem in a two-hop non-regenerative MIMO relay system with *sum* power

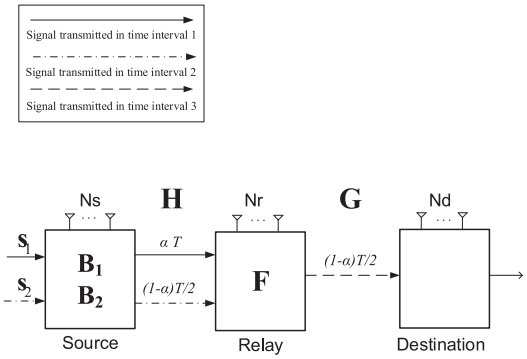

Fig. 1. A two-hop MIMO relay communication system with an energy-harvesting relay node.

constraint; (4) Practical peak power constraints at the source and relay nodes are considered during both the energy transfer and the information transfer phases; (5) The circuit power consumption at the relay node is considered in the transceiver optimization. (6) The proposed algorithms are shown to be superior to that in [2] in terms of the system MI and energy-rate trade-off, particularly in the high nominal power range, at no extra computational complexity.

D. Structure

The rest of the paper is organized as follows. The model of a two-hop non-regenerative MIMO relay system with an energy-harvesting relay node is presented in Section II. The transceiver optimization problem is also formulated in Section II. The proposed algorithms are developed in Section III. Numerical examples are presented in Section IV to demonstrate the performance of the proposed algorithms. Finally, we conclude our paper in Section V.

II. System Model

We consider a three-node two-hop MIMO communication system where the source node S transmits information to the destination node D with the aid of one relay node R as shown in Fig. 1. The source, relay, and destination nodes are equipped with N_s, N_r, and N_d antennas, respectively. We assume that the source node has its own power supply, while the relay node is powered by harvesting the RF energy sent from the source node. In particular, there are two phases in one communication cycle. In the source phase, energy-carrying and information-bearing signals are transmitted from the source node to the relay node. Then, in the relay phase, the information signals received at the relay node are linearly precoded and transmitted to the destination node [2]. Among various relaying protocols, the AF scheme is chosen at the relay node due to its implementation simplicity and shorter processing delay. Moreover, compared with other relaying protocols, the AF scheme does not need to decode and re-encode the signals at the relay node, which is energy-saving, making it suitable for wireless-powered communication. Similar to [2], [23], [24], the direct link between the source and destination nodes is not considered, as we assume that the effects of path attenuation and shadowing are more severe on the direct link compared with the link via the relay node.

We adopt the time switching protocol [5] for the energy harvesting and information transmission at the source phase. In this protocol, the total time T of one communication cycle is divided into three intervals. In the first time interval, energy is transferred from the source node to the relay node with a duration of αT, where $0 < \alpha < 1$ denotes the time switching factor. In the second time interval, information signals are transmitted from the source node to the relay node with a duration of $(1-\alpha)T/2$. The last time interval of $(1-\alpha)T/2$ is used for relaying the information signals from the relay node to the destination node. For the simplicity of presentation, we set $T = 1$ hereafter.

During the first interval, the $N_1 \times 1$ energy-carrying signal vector $\mathbf{s}_1$ is precoded by an $N_s \times N_1$ matrix $\mathbf{B}_1$ at the source node and transmitted to the relay node. The optimal value of N_1 will be determined later. We assume that $E\{\mathbf{s}_1\mathbf{s}_1^H\} = \mathbf{I}_{N_1}$, where $E\{\cdot\}$ stands for the statistical expectation, $\mathbf{I}_n$ is an $n \times n$ identity matrix, and $(\cdot)^H$ denotes the Hermitian transpose. The received signal vector at the relay node is given by

$$\mathbf{y}_{r,1} = \mathbf{H}\mathbf{B}_1\mathbf{s}_1 + \mathbf{v}_{r,1} \tag{1}$$

where $\mathbf{H}$ is an $N_r \times N_s$ MIMO channel matrix between the source and relay nodes, $\mathbf{y}_{r,1}$ and $\mathbf{v}_{r,1}$ are the received signal and the additive Gaussian noise vectors at the relay node during the first interval, respectively. Based on [5], the RF energy harvested at the relay node is proportional to the baseband received signal in (1) without the noise component, and is given by

$$E_r = \eta_1\alpha\mathrm{tr}(\mathbf{H}\mathbf{B}_1\mathbf{B}_1^H\mathbf{H}^H) \tag{2}$$

where $\mathrm{tr}(\cdot)$ denotes the matrix trace and $0 < \eta_1 \leq 1$ is the energy conversion efficiency.

During the second interval, an $N_2 \times 1$ information-bearing signal vector $\mathbf{s}_2$ with $E\{\mathbf{s}_2\mathbf{s}_2^H\} = \mathbf{I}_{N_2}$ is precoded by an $N_s \times N_2$ matrix $\mathbf{B}_2$ at the source node and transmitted to the relay node. The received signal vector at the relay node can be written as

$$\mathbf{y}_{r,2} = \mathbf{H}\mathbf{B}_2\mathbf{s}_2 + \mathbf{v}_{r,2} \tag{3}$$

where $\mathbf{v}_{r,2}$ is the additive white Gaussian noise (AWGN) vector at the relay node during the second interval with zero-mean and $E\{\mathbf{v}_{r,2}\mathbf{v}_{r,2}^H\} = \sigma_r^2\mathbf{I}_{N_r}$.

Finally, during the third interval, the relay node linearly precodes $\mathbf{y}_{r,2}$ with an $N_r \times N_r$ matrix $\mathbf{F}$ and transmits the precoded signal vector

$$\mathbf{x}_r = \mathbf{F}\mathbf{y}_{r,2} \tag{4}$$

to the destination node. From (3) and (4), the received signal vector at the destination node can be written as

$$\begin{aligned}\mathbf{y}_d &= \mathbf{G}\mathbf{x}_r + \mathbf{v}_d \\ &= \mathbf{G}\mathbf{F}\mathbf{H}\mathbf{B}_2\mathbf{s}_2 + \mathbf{G}\mathbf{F}\mathbf{v}_{r,2} + \mathbf{v}_d\end{aligned} \tag{5}$$

where $\mathbf{G}$ is an $N_d \times N_r$ MIMO channel matrix between the relay and destination nodes, $\mathbf{y}_d$ and $\mathbf{v}_d$ are the received signal vector and the AWGN vector at the destination node, respectively, with $E\{\mathbf{v}_d\mathbf{v}_d^H\} = \sigma_d^2\mathbf{I}_{N_d}$. From (5), the mutual information between source and destination is given as [12]

$$\begin{aligned}\mathrm{MI}(\alpha, \mathbf{B}_2, \mathbf{F}) = \frac{1-\alpha}{2}\log|\mathbf{I}_{N_2} + \mathbf{B}_2^H\mathbf{H}^H\mathbf{F}^H\mathbf{G}^H \\ \times(\sigma_r^2\mathbf{G}\mathbf{F}\mathbf{F}^H\mathbf{G}^H + \sigma_d^2\mathbf{I}_{N_d})^{-1}\mathbf{G}\mathbf{F}\mathbf{H}\mathbf{B}_2|\end{aligned} \tag{6}$$

where $|\cdot|$ and $(\cdot)^{-1}$ denote the matrix determinant and matrix inversion, respectively.

We assume that $\mathbf{H}$ and $\mathbf{G}$ are quasi-static and known at the relay node. We also assume that without wasting the transmission power at the source and relay nodes,

$N_2 \leq \min(\mathrm{rank}(\mathbf{H}), \mathrm{rank}(\mathbf{G}))$ and $\mathrm{rank}(\mathbf{F}) = \mathrm{rank}(\mathbf{B}_2) = N_2$, where $\mathrm{rank}(\cdot)$ stands for the rank of a matrix.

Note that the energy used to transmit $\mathbf{s}_1$ and $\mathbf{s}_2$ from the source node is $\alpha \mathrm{tr}(\mathbf{B}_1\mathbf{B}_1^H)$ and $\frac{1-\alpha}{2}\mathrm{tr}(\mathbf{B}_2\mathbf{B}_2^H)$, respectively. Therefore, the constraint on the energy consumed by the source node can be written as

$$\alpha \mathrm{tr}(\mathbf{B}_1\mathbf{B}_1^H) + \frac{1-\alpha}{2}\mathrm{tr}(\mathbf{B}_2\mathbf{B}_2^H) \leq \frac{1+\alpha}{2}P_s \tag{7}$$

where P_s is the nominal (average) power available at the source node. It is worth noting that in [2], a constant power is assumed at the source node for both energy transferring and information transmission as

$$\mathrm{tr}(\mathbf{B}_1\mathbf{B}_1^H) \leq P_s, \qquad \mathrm{tr}(\mathbf{B}_2\mathbf{B}_2^H) \leq P_s. \tag{8}$$

It can be seen that under the same α, both (7) and (8) lead to the same amount of energy consumption at the source node. However, (8) is a special case of (7) and the feasible region defined by (7) is larger than that of (8). In fact, in (7) the source precoding matrices $\mathbf{B}_1$ and $\mathbf{B}_2$ are linked through one energy constraint. This enables the source node to operate at different power levels adapted to the purpose of energy transferring at the first interval and information transmission at the second interval, which is more flexible than (8). Hence, transceivers designed under (7) are expected to have a better performance than that with (8) as in [2].

From (3) and (4), the energy consumed by the relay node to transmit $\mathbf{x}_r$ to the destination node is given by

$$\frac{1-\alpha}{2}\mathrm{tr}(E\{\mathbf{x}_r\mathbf{x}_r^H\}) = \frac{1-\alpha}{2}\mathrm{tr}(\mathbf{F}(\mathbf{H}\mathbf{B}_2\mathbf{B}_2^H\mathbf{H}^H + \sigma_r^2\mathbf{I}_{N_r})\mathbf{F}^H). \tag{9}$$

Following [32], we consider that the circuit energy consumption at the relay node contains two parts: A static part which is used to maintain the basic circuit operations and a dynamic part which depends on the amount of information processing. Considering multiple antennas at the relay node [33], we model the static part as $\frac{1-\alpha}{2}N_rP_c$, where P_c is the per-antenna static power consumption. The dynamic part[1] of the circuit energy consumption is modeled as $\eta_2 E_r$, where $0 < \eta_2 < 1$. It will be shown later that the achievable data rate increases with E_r. Thus, $\eta_2 E_r$ increases with the amount of information processing and it is sensible to adopt $\eta_2 E_r$ as the dynamic part of the circuit energy consumption. Based on (2) and (9), we obtain the following energy constraint at the relay node

$$\begin{aligned}&\frac{1-\alpha}{2}(\mathrm{tr}(\mathbf{F}(\mathbf{H}\mathbf{B}_2\mathbf{B}_2^H\mathbf{H}^H + \sigma_r^2\mathbf{I}_{N_r})\mathbf{F}^H) + N_rP_c)\\ &\quad \leq (1-\eta_2)E_r = \alpha\eta\mathrm{tr}(\mathbf{H}\mathbf{B}_1\mathbf{B}_1^H\mathbf{H}^H)\end{aligned} \tag{10}$$

where $\eta = \eta_1(1-\eta_2)$.

From (6), (7), (10), the transceiver optimization problem for two-hop non-regenerative wireless information and energy transfer MIMO relay systems can be written as

$$\max_{0<\alpha<1,\mathbf{B}_1,\mathbf{B}_2,\mathbf{F}} \ \mathrm{MI}(\alpha, \mathbf{B}_2, \mathbf{F}) \tag{11a}$$

$$\text{s.t.} \quad \alpha\mathrm{tr}(\mathbf{B}_1\mathbf{B}_1^H) + \frac{1-\alpha}{2}\mathrm{tr}(\mathbf{B}_2\mathbf{B}_2^H) \leq \frac{1+\alpha}{2}P_s \tag{11b}$$

$$\begin{aligned}&\mathrm{tr}(\mathbf{F}(\mathbf{H}\mathbf{B}_2\mathbf{B}_2^H\mathbf{H}^H + \sigma_r^2\mathbf{I}_{N_r})\mathbf{F}^H) + N_rP_c\\ &\leq \frac{2\alpha\eta}{1-\alpha}\mathrm{tr}(\mathbf{H}\mathbf{B}_1\mathbf{B}_1^H\mathbf{H}^H).\end{aligned} \tag{11c}$$

As will be shown in the next section, the energy consumption constraint greatly increases the technical difficulty of solving the problem (11) compared with the constant power constraint in [2].

III. Proposed Algorithms

The problem (11) is non-convex with matrix variables and is challenging to solve. In this section, we develop two algorithms to solve the problem (11). First, we derive the optimal structure of $\mathbf{B}_1$, $\mathbf{B}_2$, and $\mathbf{F}$, under which the problem (11) can be simplified to a power allocation problem. Let us introduce

$$\mathbf{H} = \mathbf{U}_h\mathbf{\Lambda}_h^{\frac{1}{2}}\mathbf{V}_h^H, \quad \mathbf{G} = \mathbf{U}_g\mathbf{\Lambda}_g^{\frac{1}{2}}\mathbf{V}_g^H \tag{12}$$

as the singular value decompositions (SVDs) of $\mathbf{H}$ and $\mathbf{G}$, respectively, with the diagonal elements of $\mathbf{\Lambda}_h$ and $\mathbf{\Lambda}_g$ sorted in decreasing order.

Theorem 1: The optimal $\mathbf{B}_1$, $\mathbf{B}_2$, and $\mathbf{F}$ as the solution to the problem (11) has the following structure

$$\mathbf{B}_1^* = \lambda_b^{\frac{1}{2}}\mathbf{v}_{h,1}, \quad \mathbf{B}_2^* = \mathbf{V}_{h,1}\mathbf{\Lambda}_2^{\frac{1}{2}}, \quad \mathbf{F}^* = \mathbf{V}_{g,1}\mathbf{\Lambda}_f^{\frac{1}{2}}\mathbf{U}_{h,1}^H \tag{13}$$

where $(\cdot)^*$ stands for the optimal value, λ_b is a positive scalar, $\mathbf{v}_{h,1}$ is the first column of $\mathbf{V}_h$, $\mathbf{\Lambda}_2$ and $\mathbf{\Lambda}_f$ are $N_2 \times N_2$ diagonal matrices, $\mathbf{V}_{g,1}$, $\mathbf{U}_{h,1}$, and $\mathbf{V}_{h,1}$ contain the leftmost N_2 columns from $\mathbf{V}_g$, $\mathbf{U}_h$, and $\mathbf{V}_h$, respectively.

Proof: See Appendix A. ■

It is interesting to see from (13) that the optimal $\mathbf{B}_1$ is a vector (i.e., $N_1 = 1$) matching $\mathbf{v}_{h,1}$. This indicates that in order to maximize the energy harvested by the relay node, all transmission power at the source node should be allocated to the channel corresponding to the largest singular value of $\mathbf{H}$ during the first interval. As a result, we only need to optimize λ_b in $\mathbf{B}_1$, and the transmission power of the source during the first interval is $\mathrm{tr}(\mathbf{B}_1\mathbf{B}_1^H) = \lambda_b$. It can also be seen from (13) that the optimal structure of $\mathbf{B}_2$ and $\mathbf{F}$ is similar to that in two-hop MIMO relay systems where the relay node has self-power supply [13].

By substituting (13) back into (11), the transceiver optimization problem (11) with matrix variables is simplified to the following power allocation problem with scalar variables

$$\max_{\alpha,\lambda_b,\boldsymbol{\lambda}_2,\boldsymbol{\lambda}_f} \ \frac{1-\alpha}{2}\sum_{i=1}^{N_2}\log\left(1 + \frac{\lambda_{2,i}\lambda_{h,i}\lambda_{f,i}\lambda_{g,i}}{1+\lambda_{f,i}\lambda_{g,i}}\right) \tag{14a}$$

$$\text{s.t.} \quad \alpha\lambda_b + \frac{1-\alpha}{2}\sum_{i=1}^{N_2}\lambda_{2,i} \leq \frac{1+\alpha}{2}P_s \tag{14b}$$

$$\sum_{i=1}^{N_2}\lambda_{f,i}(\lambda_{h,i}\lambda_{2,i}+1) \leq \frac{2\alpha\eta}{1-\alpha}\tilde{\lambda}_{h,1}\lambda_b - N_rP_c \tag{14c}$$

$$0 < \alpha < 1, \ \lambda_{f,i} \geq 0, \ \lambda_{2,i} \geq 0, i = 1, \ldots, N_2 \tag{14d}$$

where $\boldsymbol{\lambda}_2 = [\lambda_{2,1}, \ldots, \lambda_{2,N_2}]^T$, $\boldsymbol{\lambda}_f = [\lambda_{f,1}, \ldots, \lambda_{f,N_2}]^T$, $\lambda_{h,i} = \tilde{\lambda}_{h,i}/\sigma_r^2$, $\lambda_{g,i} = \tilde{\lambda}_{g,i}/\sigma_d^2$, $\lambda_{f,i} = \tilde{\lambda}_{f,i}\sigma_r^2$, $\lambda_{2,i}$, $\tilde{\lambda}_{f,i}$, $\tilde{\lambda}_{h,i}$, $\tilde{\lambda}_{g,i}$

[1] We assume that all the energy harvested at the relay node E_r is consumed for the purpose of relaying signals from the source node to the destination node. In [32], the dynamic part of the circuit power consumption is modeled as ξR, where R is the data rate and ξ is a constant representing the dynamic power consumption per unit data rate. Note that adopting this model will make the resulting problem (11) intractable as the objective function (11a) will appear in the constraint (11c).

denote the ith diagonal element of $\mathbf{\Lambda}_2$, $\mathbf{\Lambda}_f$, $\mathbf{\Lambda}_h$ and $\mathbf{\Lambda}_g$, respectively. Note that the feasibility of the problem (14) can be guaranteed by a proper choice of P_s as shown later. By introducing $z_i = \lambda_{f,i}(\lambda_{h,i}\lambda_{2,i}+1), i = 1, \ldots, N_2$, the problem (14) becomes

$$\max_{\alpha,\lambda_b,\boldsymbol{\lambda}_2,\mathbf{z}} \quad \frac{1-\alpha}{2}\sum_{i=1}^{N_2}\log\left(1+\frac{\lambda_{2,i}\lambda_{h,i}z_i\lambda_{g,i}}{1+\lambda_{2,i}\lambda_{h,i}+z_i\lambda_{g,i}}\right) \tag{15a}$$

$$\text{s.t.} \quad \alpha\lambda_b + \frac{1-\alpha}{2}\sum_{i=1}^{N_2}\lambda_{2,i} \le \frac{1+\alpha}{2}P_s \tag{15b}$$

$$\sum_{i=1}^{N_2} z_i \le \frac{2\alpha\eta}{1-\alpha}\tilde{\lambda}_{h,1}\lambda_b - N_r P_c \tag{15c}$$

$$0<\alpha<1,\ \lambda_{2,i}\ge 0,\ z_i \ge 0,\ i=1,\ldots,N_2 \tag{15d}$$

where $\mathbf{z} = [z_1, \ldots, z_{N_2}]^T$.

As for any λ_b, the optimal $\mathbf{z}$ maximizing (15a) must satisfy equality in (15c), i.e.,

$$\sum_{i=1}^{N_2} z_i = \frac{2\alpha\eta}{1-\alpha}\tilde{\lambda}_{h,1}\lambda_b - N_r P_c. \tag{16}$$

Using (16), the problem (15) can be equivalently rewritten as

$$\max_{\alpha,\boldsymbol{\lambda}_2,\mathbf{z}} \quad \frac{1-\alpha}{2}\sum_{i=1}^{N_2}\log\left(1+\frac{\lambda_{2,i}\lambda_{h,i}z_i\lambda_{g,i}}{1+\lambda_{2,i}\lambda_{h,i}+z_i\lambda_{g,i}}\right) \tag{17a}$$

$$\text{s.t.} \quad \frac{1-\alpha}{2\eta\tilde{\lambda}_{h,1}}\left(\sum_{i=1}^{N_2} z_i + N_r P_c\right) + \frac{1-\alpha}{2}\sum_{i=1}^{N_2}\lambda_{2,i} \le \frac{1+\alpha}{2}P_s \tag{17b}$$

$$0<\alpha<1, \quad \lambda_{2,i}\ge 0, \quad z_i \ge 0,\ i=1,\ldots,N_2. \tag{17c}$$

By introducing $a_i = \lambda_{h,i}$, $b_i = \eta\sigma_r^2\lambda_{g,i}\lambda_{h,1}$, $x_i = \lambda_{2,i}$, $y_i = z_i/(\eta\tilde{\lambda}_{h,1})$, $i = 1, \ldots, N_2$, the problem (17) becomes

$$\min_{\alpha,\mathbf{x},\mathbf{y}} \quad \frac{1-\alpha}{2}\sum_{i=1}^{N_2}\log\frac{1+a_ix_i+b_iy_i}{(1+a_ix_i)(1+b_iy_i)} \tag{18a}$$

$$\text{s.t.} \quad \sum_{i=1}^{N_2} x_i + \sum_{i=1}^{N_2} y_i \le P_s\frac{1+\alpha}{1-\alpha} - P_0 \tag{18b}$$

$$0<\alpha<1, \quad x_i\ge 0, \quad y_i \ge 0, \quad i=1,\ldots,N_2 \tag{18c}$$

where $\mathbf{x} = [x_1, \ldots, x_{N_2}]^T$, $\mathbf{y} = [y_1, \ldots, y_{N_2}]^T$, and $P_0 = \frac{N_r P_c}{\eta\tilde{\lambda}_{h,1}}$. We assume that the static part of the circuit power consumption $N_r P_c < \eta\tilde{\lambda}_{h,1}P_s$ such that $P_s\frac{1+\alpha}{1-\alpha} - P_0 > 0$ for $0<\alpha<1$. This can be satisfied by adjusting P_s. Interestingly, although the problem (18) is still a non-convex optimization problem, it has a nice symmetric structure with respect to $\mathbf{x}$ and $\mathbf{y}$ in both the objective function (18a) and the constraint (18b).

Let $M(\alpha)$ be the optimal value of the problem (19) with a given α written as

$$\min_{\mathbf{x},\mathbf{y}} \quad \sum_{i=1}^{N_2}\log\frac{1+a_ix_i+b_iy_i}{(1+a_ix_i)(1+b_iy_i)} \tag{19a}$$

$$\text{s.t.} \quad \sum_{i=1}^{N_2} x_i + \sum_{i=1}^{N_2} y_i \le P_\alpha \tag{19b}$$

$$x_i \ge 0, \quad y_i \ge 0, \quad i=1,\ldots,N_2 \tag{19c}$$

Algorithm 1: Applying the Golden Section Search to Find the Optimal α and the Precoding Matrices.

Input: P_s, a_i, b_i, $i = 1, \ldots, N_2$.
Output: α^*, $\mathbf{B}_1^*$, $\mathbf{B}_2^*$, and $\mathbf{F}^*$.

Initialization: $\alpha_l = 0$ and $\alpha_u = 1$.
while $|\alpha_u - \alpha_l| > \varepsilon$ **do**
  Define $c_1 = (\delta-1)\alpha_l + (2-\delta)\alpha_u$ and $c_2 = (2-\delta)\alpha_l + (\delta-1)\alpha_u$.
  Solve the problem (19) for $\alpha = c_1$ by optimizing $\mathbf{x}$ and $\mathbf{y}$ through the primal decomposition based algorithm (Algorithm 2) in Sections III-A and III-B or the upper bound based algorithm (Algorithm 4) in Section III-C, and return $M(c_1)$;
  Compute $F(c_1) = \frac{1-c_1}{2}M(c_1)$.
  Repeat Step 3 for $\alpha = c_2$.
  if $F(c_1) < F(c_2)$ **then**
    Assign $\alpha_u = c_2$.
  else
    Assign $\alpha_l = c_1$.
  end if
end while
$\alpha^* = (\alpha_u + \alpha_l)/2$.
Calculate the optimal $\mathbf{B}_1^*$, $\mathbf{B}_2^*$, and $\mathbf{F}^*$ based on (13) where

$$\lambda_b^* = \frac{1-\alpha^*}{2\alpha^*}\left(\sum_{i=1}^{N_2} y_i^* + P_0\right),\ \lambda_{2,i}^* = x_i^*,\ \tilde{\lambda}_{f,i}^* = \frac{y_i^*\tilde{\lambda}_{h,1}\eta}{(\lambda_{h,i}x_i^*+1)\sigma_r^2}.$$

where

$$P_\alpha = P_s\frac{1+\alpha}{1-\alpha} - P_0. \tag{20}$$

Then the objective function (18a) can be written as $F(\alpha) = \frac{1-\alpha}{2}M(\alpha)$. From (20), we know that P_α monotonically increases with α. Thus, it can be seen from (19b) that the feasible region of the problem (19) expands as α increases. Therefore, $M(\alpha)$ monotonically decreases as α increases. On the other hand, $1-\alpha$ monotonically decreases as α increases. Considering the effects of α on $M(\alpha)$ and $1-\alpha$, and the fact that $M(\alpha) < 0$, we can expect that $F(\alpha)$ is a unimodal function of α.

The unimodality of $F(\alpha)$ is difficult to prove rigorously[2] for $N_2 > 1$, and it will be illustrated graphically in Section III-A. Based on this observation, the problem (18) can be efficiently solved by a two-loop algorithm, where for a given α we optimize $\mathbf{x}$ and $\mathbf{y}$ by solving the problem (19). And then a simple one dimensional search (such as the golden section search method [30]) can be applied to obtain the optimal α. The procedure of the proposed two-loop algorithm is summarized in Algorithm 1, where ε is a positive constant close to 0, and $\delta > 0$ is the reduction factor.[3] It is shown in [30] that the optimal $\delta = 1.618$, also known as the golden ratio. Finally, the optimal precoding matrices are obtained as Step 12 in Algorithm 1.

[2]The difficulty is that for $N_2 > 1$, α changes the value of $M(\alpha)$ through varying the feasible region of $\mathbf{x}$ and $\mathbf{y}$ of the optimization problem (19), and the objective function (19a) is a complicated function of $\mathbf{x}$ and $\mathbf{y}$. As a result, the closed-form expression of $F(\alpha)$ is difficult to obtain.

[3]Algorithm 1 can be viewed as an iterative algorithm where the problem (18) is solved by alternatingly updating α and $(\mathbf{x}, \mathbf{y})$.

Interestingly, the problem (19) can be viewed as a power allocation problem for a two-hop non-regenerative MIMO relay system with sum power constraint across the source and relay nodes. In the next subsections, we propose two algorithms to solve the problem (19). The first algorithm is based on the primal decomposition technique [31], and provides a globally optimal solution to the problem (19). This is an important novel contribution of our work. To the best of our knowledge, the globally optimal solution to the problem (19) is obtained for the first time in this work. The second algorithm exploits a tight upper bound of (19a), which yields a slightly worse performance but has a much lower computational complexity than the primal decomposition based algorithm. Such performance-complexity tradeoff is very useful in practical MIMO relay systems with an energy-harvesting relay node.

A. Primal Decomposition Based Algorithm

We observe that in (19a) and (19b), each pair of x_i and y_i are decoupled from the other pairs. This indicates that the problem (19) can be efficiently solved by a primal decomposition method [31], where each pair of x_i and y_i, $i = 1, \ldots, N_2$, are optimized through solving the subproblem of

$$\min_{x_i, y_i} \ \log \frac{1 + a_i x_i + b_i y_i}{(1 + a_i x_i)(1 + b_i y_i)} \tag{21a}$$

$$\text{s.t. } x_i + y_i = p_i, \quad x_i \geq 0, \quad y_i \geq 0. \tag{21b}$$

Here the N_2 subproblems of (21) are linked through nonnegative p_i by the constraint of $\sum_{i=1}^{N_2} p_i \leq P_\alpha$. By substituting $y_i = p_i - x_i$ back into (21a), we have

$$g_i(x_i) = \log \frac{1 + a_i x_i + b_i (p_i - x_i)}{(1 + a_i x_i)(1 + b_i (p_i - x_i))}.$$

Based on the first-order optimality condition of $\partial g_i / \partial x_i = 0$ and $x_i \geq 0$, we obtain a closed-form solution of x_i to the problem (21) as

$$x_i^* = \frac{\sqrt{b_i p_i + 1}}{a_i - b_i} (\sqrt{a_i p_i + 1} - \sqrt{b_i p_i + 1}). \tag{22}$$

From $y_i = p_i - x_i$, the optimal y_i is given by

$$y_i^* = \frac{\sqrt{a_i p_i + 1}}{a_i - b_i} (\sqrt{a_i p_i + 1} - \sqrt{b_i p_i + 1}). \tag{23}$$

Interestingly, from (22) and (23), we find that $y_i^*/x_i^* = \sqrt{a_i p_i + 1}/\sqrt{b_i p_i + 1}$.

Let us introduce

$$f_i(p_i) = \log \frac{1 + a_i x_i^* + b_i y_i^*}{(1 + a_i x_i^*)(1 + b_i y_i^*)} \tag{24}$$

$$= 2 \log \frac{a_i - b_i}{a_i \sqrt{b_i p_i + 1} - b_i \sqrt{a_i p_i + 1}} \tag{25}$$

where (25) is obtained by substituting x_i^* in (22) and y_i^* in (23) into (24). The master problem of optimizing $\mathbf{x}$ and $\mathbf{y}$ in (19) can be written as the following power allocation problem

$$\min_{\mathbf{p}} \ \sum_{i=1}^{N_2} f_i(p_i) \tag{26a}$$

$$\text{s.t. } \sum_{i=1}^{N_2} p_i \leq P_\alpha, \quad p_i \geq 0, \quad i = 1, \ldots, N_2 \tag{26b}$$

Algorithm 2: Solving the Problem (19) Using the Proposed Primal Decomposition Based Algorithm.

Input: P_α, a_i, b_i, $i = 1, \ldots, N_2$.
Output: x_i^*, y_i^*, $i = 1, \ldots, N_2$.
1: Solve (27) and (31) using the approach in Algorithm 3 to obtain the optimal p_i^*, $i = 1, \ldots, N_2$.
2: Compute the optimal $\mathbf{x}^*$ and $\mathbf{y}^*$ as (22) and (23) with p_i^*, $i = 1, \ldots, N_2$.

where $\mathbf{p} = [p_1, \ldots, p_{N_2}]^T$.

The master problem (26) can be solved by the Lagrange multiplier method. The Lagrangian function is given by $L(\mathbf{p}, \mu) = \sum_i^{N_2} f_i(p_i) + \mu \left(\sum_{i=1}^{N_2} p_i - P_\alpha \right)$, where $\mu \geq 0$ is the Lagrange multiplier. From the Karush-Kuhn-Tucker (KKT) optimality conditions [34], we have

$$\frac{\partial L}{\partial p_i} = -\frac{\mu_2(p_i, a_i, b_i)}{\mu_1(p_i, a_i, b_i)} + \mu = 0, \quad i = 1, \ldots, N_2 \tag{27}$$

$$\mu \left(\sum_{i=1}^{N_2} p_i - P_\alpha \right) = 0 \tag{28}$$

where

$$\mu_1(p_i, a_i, b_i) = \sqrt{(a_i p_i + 1)(b_i p_i + 1)} \tag{29}$$

$$\mu_2(p_i, a_i, b_i) = \frac{a_i b_i (\sqrt{a_i p_i + 1} - \sqrt{b_i p_i + 1})}{a_i \sqrt{b_i p_i + 1} - b_i \sqrt{a_i p_i + 1}}. \tag{30}$$

By solving the nonlinear equation (27), we obtain p_i as a function of μ denoted as $p_i(\mu)$. Moreover, it can be seen from (27) and (30) that as $a_i \neq b_i$, there is $\mu \neq 0$. Thus, from (28), we can obtain μ and hence the optimal p_i^* of the master problem (26) by solving the following nonlinear equation

$$\sum_{i=1}^{N_2} p_i(\mu) - P_\alpha = 0. \tag{31}$$

The procedure of using the proposed primal decomposition based algorithm to solve the problem (19) is summarized in Algorithm 2.

Using the primal decomposition based algorithm, we have $M(\alpha) = \sum_{i=1}^{N_2} f_i(p_i^*)$ and thus $F(\alpha) = \frac{1-\alpha}{2} \sum_{i=1}^{N_2} f_i(p_i^*)$, where p_i^*, $i = 1, \ldots, N_2$, is the optimal solution to the problem (26). To verify the unimodality of $F(\alpha)$, we first study the special case of $N_2 = 1$. In this case, we do not need to solve the master power allocation problem (26) and a closed-form expression of $F(\alpha)$ can be obtained from (25) as

$$F(\alpha) = \frac{1 - \alpha}{2} f_1(P_\alpha)$$

$$= (1 - \alpha) \log \frac{a_1 - b_1}{a_1 \sqrt{b_1 P_\alpha + 1} - b_1 \sqrt{a_1 P_\alpha + 1}}. \tag{32}$$

The first-order derivative of $F(\alpha)$ is given by

$$F'(\alpha) = -\log \frac{a_1 - b_1}{a_1 \sqrt{b_1 P_\alpha + 1} - b_1 \sqrt{a_1 P_\alpha + 1}} - \frac{\frac{a_1 b_1 P_s}{1 - \alpha} \left(\frac{1}{\sqrt{b_1 P_\alpha + 1}} - \frac{1}{\sqrt{a_1 P_\alpha + 1}} \right)}{a_1 \sqrt{b_1 P_\alpha + 1} - b_1 \sqrt{a_1 P_\alpha + 1}}. \tag{33}$$

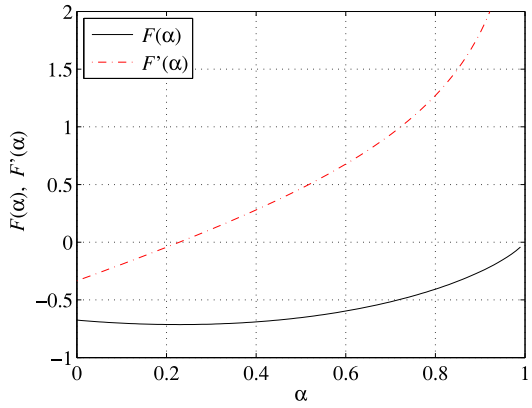

Fig. 2. Unimodality of $F(\alpha)$ with $N_2 = 1$.

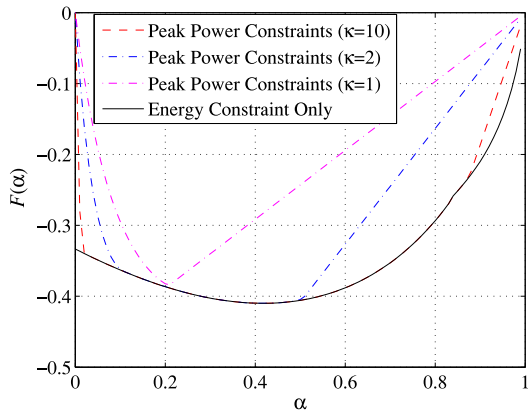

Fig. 3. Unimodality of $F(\alpha)$ with $N_2 = 3$.

Fig. 2 shows the value of (32) and (33) versus α with $P_s = 5$ dBm and $N_s = N_r = N_d = N_2 = 1$. It can be clearly seen that as $F'(\alpha)$ crosses zero only once, $F(\alpha)$ in (32) is a unimodal function of α.

For the general case of $N_2 > 1$, a closed-form expression of $F(\alpha)$ is not available. Nevertheless, we can solve the problem (26) through (27) and (31) to calculate $F(\alpha)$ numerically. The 'Energy Constraint Only' curve in Fig. 3 shows $F(\alpha)$ versus α at $P_s = 0$ dBm with $N_s = N_r = N_d = N_2 = 3$ calculated using the primal decomposition based algorithm described above. It can be observed that $F(\alpha)$ is a unimodal function of α.

We would like to note that it is non-trivial to solve (27) and (31). This is because it is difficult to express p_i explicitly as a function of μ from (27). Moreover, μ is not a monotonic function of p_i in (27). In the next subsection, we develop an efficient algorithm to solve (27) and (31) and thus obtain the global optimum $p_i, i = 1, \ldots, N_2$, by exploring the structure of (27) and the principle of water-filling.

B. Solving Nonlinear Equations (27) and (31)

Lemma 1: For each i in (27)

$$\mu(p_i, a_i, b_i) = \frac{\mu_2(p_i, a_i, b_i)}{\mu_1(p_i, a_i, b_i)} \tag{34}$$

is a unimodal function of $p_i \geq 0$, and monotonically increases with $a_i \geq 0$ and $b_i \geq 0$.

Proof: See Appendix B. ■

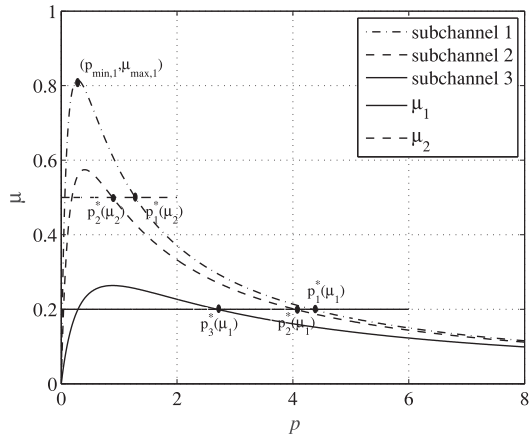

Fig. 4. Unimodality of $\mu(p_i)$ with $N_s = N_r = N_d = N_2 = 3$.

We plot $\mu(p_i, a_i, b_i)$ in Fig. 4 versus p where $N_s = N_r = N_d = N_2 = 3$, and for subchannels 1–3, there are $(a_1, b_1) = (3.396, 14.843)$, $(a_2, b_2) = (2.748, 6.463)$, and $(a_3, b_3) = (0.928, 2.647)$. It can be clearly seen from Fig. 4 that for all subchannels, μ is a unimodal function of p_i. It can be easily shown from (34) that $\mu(p_i = 0) = \mu(p_i = \infty) = 0$. We can also observe from Fig. 4 that for any p, the value of μ decreases with the subchannel index i ($i = 1$ corresponds to the strongest spatial subchannel having the largest (a_i, b_i), whereas $i = 3$ is the weakest one with the smallest (a_i, b_i)). This supports the statement in Lemma 1 that μ is a monotonically increasing function of a_i and b_i.

We would like to note that the difficulties in solving the power allocation problem (27) and (31) are two-folds. First, there is no closed-form solution to (27). Second, it can be seen from Fig. 4 that for the ith subchannel, there are two roots with a given μ for $\mu < \mu_{\max,i}$ (i.e., the peak point).

By taking a closer look at (27) and (31), we find that they can be solved by resorting to the principle of water-filling. In particular, μ can be viewed as the 'water level' which should be properly chosen to satisfy the power constraint (31). Moreover, for a given μ, considering that $f_i(p_i)$ decreases with p_i, the larger root between the two roots (the root on the right) should be chosen in order to minimize (26a), as shown in Fig. 4.

Since μ is a monotonically increasing function of a_i and b_i, for each μ, the value of the solution p_i^* to the ith problem in (27) decreases with i, i.e., $p_1^*(\mu_1) > p_2^*(\mu_1) > p_3^*(\mu_1)$ and $p_1^*(\mu_2) > p_2^*(\mu_2)$ as illustrated in Fig. 4. This agrees with the well-known water-filling principle, where more power should be allocated to stronger subchannels (with a larger (a_i, b_i)), in order to maximize the system MI.

We can also observe from Fig. 4 that if P_α in (31) is large enough, then all three subchannels have non-zero power. An example of this case corresponds to the water level μ_1 where $p_1^*(\mu_1) + p_2^*(\mu_1) + p_3^*(\mu_1) = P_\alpha$. Once the power P_α available is not enough for all three subchannels, following the principle of water-filling, the weakest subchannels do not get any power allocation. This situation is illustrated by water level μ_2 where subchannel 3 has zero power and $p_1^*(\mu_2) + p_2^*(\mu_2) = P_\alpha$. If the power P_α is very small such that $P_\alpha \leq p_{\min,1}$, where $p_{\min,1}$ is the power associated with the peak point of the strongest subchannel shown on Fig. 4, then following the water-filling principle, we have $p_1^* = P_\alpha$ and $p_i^* = 0, i = 2, \ldots, N_2$.

Based on the discussions above, we develop an efficient algorithm to solve (27) and (31) as summarized in Algorithm 3. This algorithm has two stages if $P_\alpha > p_{\min,1}$. At the initialization stage, we determine the set of subchannels $\mathcal{I} = [1, \ldots, L]$ ($L \leq N_2$) that have non-zero power allocation. Whereas at the main stage, we obtain the optimal μ and p_i, $i = 1, \ldots, L$, that satisfy (27) and (31) through a two-loop bisection search, based on the fact that p_i monotonically decreases with μ for $p_i \geq p_{\min,i}$, where $p_{\min,i}$ is the p_i associated with the maximal μ for the ith subchannel as shown in Fig. 4. It can be seen from Algorithm 2 and Algorithm 3 that the complexity of the primal decomposition based algorithm can be estimated as $\mathcal{O}((c_0 + c_1 c_2) N_2)$, where c_0 is the number of iterations required to determine $\mathcal{I}$ at the initialization stage, c_1 and c_2 stand for the number of iterations in the outer and inner bi-section loops, respectively, at the main stage to obtain the optimal p_i.

Theorem 2: The primal decomposition based algorithm obtains the globally optimal solution of the problem (19).

Proof: Firstly, as x_i^* in (22) is the only $x_i \geq 0$ that satisfies the first-order optimality condition of $\partial g_i / \partial x_i = 0$, (22) and (23) are the globally optimal solution to the subproblem (21).

Secondly, as constraints in (26b) are linear constraints, from the linearity constraint qualification [35], the optimal primal variables p_i, $i = 1, \ldots, N_2$ and the optimal dual variable μ of the master problem (26) must satisfy the KKT conditions (27) and (28). By exploiting the property of $\mu(p_i, a_i, b_i)$ in Lemma 1 and using the water-filling principle, we choose the proper root of p_i in (27). Therefore, among any possible solutions to (27) and (31), the solution obtained by Algorithm 3 is globally optimal to the master problem (26).

In summary, since the globally optimal p_i, $i = 1, \ldots, N_2$ are obtained from the solution of the master problem (26), and for each p_i, the globally optimal x_i and y_i are found, the primal decomposition based algorithm obtains the globally optimal solution of the problem (19). ■

Algorithm 3: Solving the Equations (27) and (31).

Input: P_α, a_i, b_i, $i = 1, \ldots, N_2$.
Output: p_i^*, $i = 1, \ldots, N_2$.

if $P_\alpha \leq p_{\min,1}$ **then**
  Set $p_1^* = P_\alpha$ and $p_i^* = 0$, $i = 2, \ldots, N_2$.
else
  Initialization stage:
  Identify the maximal point $(p_{\min,i}, \mu_{\max,i})$ of $\mu(p_i)$ for each $i \in \mathcal{I}$, where $\mathcal{I} = \{1, \ldots, N_2\}$.
  if $p_{\min,i} \geq P_\alpha$, $i = 2, \ldots, N_2$ **then**
    Remove i from $\mathcal{I}$.
  end if
  Set $\mu_{\max} = \min_{i \in \mathcal{I}} \{\mu_{\max,i}\}$. Solve p_i for each $i \in \mathcal{I}$ in (27) with $\mu = \mu_{\max}$ through a bisection search over the interval of $[p_{\min,i}, p_{\max,i}]$, where $p_{\max,i}$ is a sufficiently large number.
  if $\sum_{i \in \mathcal{I}} p_i \leq P_\alpha$ **then**
    Goto Step 15.
  else
    Remove i that corresponds to the smallest (a_i, b_i) from $\mathcal{I}$ and go back to Step 9.
  end if
  Main stage:
  Set $\mu_{\min} = 0$.
  while $\mu_{\max} - \mu_{\min} > \varepsilon$ **do**
    Let $\mu = (\mu_{\max} + \mu_{\min})/2$. Find p_i^* in (27) for each $i \in \mathcal{I}$ through a bisection search over the interval of $[p_{\min,i}, p_{\max,i}]$.
    if $\sum_{i \in \mathcal{I}} p_i^* \leq P_\alpha$ **then**
      Set $\mu_{\max} = \mu$.
    else
      Set $\mu_{\min} = \mu$.
    end if
  end while
end if

C. Upper Bound Based Algorithm

The primal decomposition based algorithm requires a two-loop bisection search, which may have a high computational complexity. In this subsection, we propose an algorithm to solve the problem (19) based on a tight upper bound of (19a), which has a lower computational complexity than the primal decomposition based algorithm. The idea of this algorithm is to introduce the following upper bound

$$\frac{1 + a_i x_i + b_i y_i}{(1 + a_i x_i)(1 + b_i y_i)} < \frac{1 + a_i x_i + b_i y_i + 1}{(1 + a_i x_i)(1 + b_i y_i)} = \frac{1}{1 + a_i x_i} + \frac{1}{1 + b_i y_i}. \tag{35}$$

Using (35), the problem of optimizing $\mathbf{x}$ and $\mathbf{y}$ with a given α can be written as

$$\min_{\mathbf{x},\mathbf{y}} \sum_{i=1}^{N_2} \log\left(\frac{1}{1 + a_i x_i} + \frac{1}{1 + b_i y_i}\right) \tag{36a}$$

$$\text{s.t.} \sum_{i=1}^{N_2} x_i + \sum_{i=1}^{N_2} y_i \leq P_\alpha \tag{36b}$$

$$x_i \geq 0, \quad y_i \geq 0, \quad i = 1, \ldots, N_2. \tag{36c}$$

The problem (36) is convex and can be efficiently solved by the Lagrange multiplier method. The Lagrangian function of (36) is

$$L(\mathbf{x}, \mathbf{y}, \nu) = \sum_{i=1}^{N_2} \log\left(\frac{1}{1 + a_i x_i} + \frac{1}{1 + b_i y_i}\right) + \nu\left(\sum_{i=1}^{N_2} x_i + \sum_{i=1}^{N_2} y_i - P_\alpha\right) \tag{37}$$

where $\nu \geq 0$ is the Lagrange multiplier.

Considering the KKT conditions, we have from (37) that for $i = 1, \ldots, N_2$

$$\frac{\partial L}{\partial x_i} = -\left(\frac{1}{1 + a_i x_i} + \frac{1}{1 + b_i y_i}\right)^{-1} \frac{a_i}{(1 + a_i x_i)^2} + \nu = 0 \tag{38}$$

$$\frac{\partial L}{\partial y_i} = -\left(\frac{1}{1 + a_i x_i} + \frac{1}{1 + b_i y_i}\right)^{-1} \frac{b_i}{(1 + b_i y_i)^2} + \nu = 0. \tag{39}$$

From (38) and (39), we obtain the following equation

$$\frac{a_i}{(1 + a_i x_i)^2} = \frac{b_i}{(1 + b_i y_i)^2}, \quad i = 1, \ldots, N_2. \tag{40}$$

By substituting (40) back into (38) and (39) and considering that $x_i \geq 0$ and $y_i \geq 0$, the optimal x_i^* and y_i^* can be obtained as

$$x_i^* = \left[\frac{\sqrt{b_i}}{\left(\sqrt{a_i}+\sqrt{b_i}\right)\nu} - \frac{1}{a_i}\right]^\dagger, \quad i = 1, \ldots, N_2 \tag{41}$$

$$y_i^* = \left[\frac{\sqrt{a_i}}{\left(\sqrt{a_i}+\sqrt{b_i}\right)\nu} - \frac{1}{b_i}\right]^\dagger, \quad i = 1, \ldots, N_2 \tag{42}$$

where for a real-valued number x, $[x]^\dagger = \max(x, 0)$.

The Lagrange multiplier ν can be computed by solving the following nonlinear equation

$$\sum_{i=1}^{N_2}(x_i^* + y_i^*) = P_\alpha \tag{43}$$

where x_i^* and y_i^* are given in (41) and (42), respectively. As the left hand side of (43) is monotonically decreasing with respect to ν, (43) can be efficiently solved by the bisection method [34]. Interestingly, when P_α is sufficiently large, for $i = 1, \ldots, N_2$, there is

$$x_i^* = \frac{\sqrt{b_i}}{\left(\sqrt{a_i}+\sqrt{b_i}\right)\nu} - \frac{1}{a_i}, \quad y_i^* = \frac{\sqrt{a_i}}{\left(\sqrt{a_i}+\sqrt{b_i}\right)\nu} - \frac{1}{b_i}. \tag{44}$$

Substituting (44) back into (43), we obtain ν as

$$\nu = N_2/Q_\alpha \tag{45}$$

where $Q_\alpha = P_\alpha + \sum_{i=1}^{N_2}(\frac{1}{a_i} + \frac{1}{b_i})$. Substituting (45) back into (44), we obtain for $i = 1, \ldots, N_2$

$$x_i^* = \frac{\sqrt{b_i}Q_\alpha}{(\sqrt{a_i}+\sqrt{b_i})N_2} - \frac{1}{a_i}, \quad y_i^* = \frac{\sqrt{a_i}Q_\alpha}{(\sqrt{a_i}+\sqrt{b_i})N_2} - \frac{1}{b_i}. \tag{46}$$

Theorem 3: The upper bound based objective function

$$F_1(\alpha) = \frac{1-\alpha}{2}\sum_{i=1}^{N_2}\log\left(\frac{1}{1+a_i x_i^*} + \frac{1}{1+b_i y_i^*}\right) \tag{47}$$

with x_i^* and y_i^* given by (46), is a strictly convex function of $0 < \alpha < 1$.

Proof: Substituting (46) back into (36a) we have

$$\begin{aligned} M_1(\alpha) &= \sum_{i=1}^{N_2}\log\left(\frac{1}{1+a_i x_i^*} + \frac{1}{1+b_i y_i^*}\right) \\ &= \chi - N_2\log\left(P_s\frac{1+\alpha}{1-\alpha} + \tau\right) \end{aligned} \tag{48}$$

where

$$\tau = \sum_{i=1}^{N_2}\left(\frac{1}{a_i}+\frac{1}{b_i}\right) - P_0, \quad \chi = \sum_{i=1}^{N_2}\log\frac{(\sqrt{a_i}+\sqrt{b_i})^2 N_2}{a_i b_i}.$$

From (48), we have the first-order and second-order derivatives of $M_1(\alpha)$ as

$$M_1'(\alpha) = \frac{2P_s N_2}{(\alpha-1)[(P_s+\tau)+(P_s-\tau)\alpha]} \tag{49}$$

$$M_1''(\alpha) = -\frac{4P_s N_2[\alpha P_s + (1-\alpha)\tau]}{(\alpha-1)^2[(P_s+\tau)+(P_s-\tau)\alpha]^2}. \tag{50}$$

Algorithm 4: Solving the Problem (19) Using the Proposed Upper Bound Based Algorithm.

Input: $P_\alpha, a_i, b_i, i = 1, \ldots, N_2$.
Output: $x_i^*, y_i^*, i = 1, \ldots, N_2$.
Initialization: The lower bound ν_l and the upper bound ν_u of ν; Set $x_i^* = y_i^* = 0$, $i = 1, \ldots, N_2$.
while $|\sum_{i=1}^{N_2}(x_i^* + y_i^*) - P_\alpha| > \epsilon$ **do**
  Set $\nu = (\nu_l + \nu_u)/2$.
  Update $\mathbf{x}^*$ as (41) and $\mathbf{y}^*$ as (42).
  if $\sum_{i=1}^{N_2}(x_i^* + y_i^*) - P_\alpha > \epsilon$ **then**
    Set $\nu_l = \nu$.
  else
    Set $\nu_u = \nu$.
  end if
end while

We obtain from (47)–(50) that $F_1(\alpha) = \frac{1-\alpha}{2}M_1(\alpha)$ and the second-order derivative of $F_1(\alpha)$ as

$$\begin{aligned} F_1''(\alpha) &= \frac{1}{2}[(1-\alpha)M_1''(\alpha) - 2M_1'(\alpha)] \\ &= \frac{2P_s^2 N_2}{(1-\alpha)[(P_s+\tau)+(P_s-\tau)\alpha]^2}. \end{aligned} \tag{51}$$

Obviously, (51) indicates that $F_1''(\alpha) > 0$ for $0 < \alpha < 1$. Thus, $F_1(\alpha)$ is a strictly convex function of $0 < \alpha < 1$. ■

The procedure of using the proposed upper bound based algorithm to solve the problem (19) is summarized in Algorithm 4. As only a one-loop bisection search is needed, the upper bound based algorithm has a complexity order of $\mathcal{O}(c_3 N_2)$, where c_3 is the number of bisection search used. We observed during simulations that c_3 is much smaller than $c_0 + c_1 c_2$. Therefore, the upper bound based algorithm has a lower computational complexity than the primal decomposition based approach. It will be shown in Section IV that compared with the primal decomposition based algorithm, the upper bound based approach has a negligible performance loss.

As the complexity of calculating the SVD of $\mathbf{H}$ and $\mathbf{G}$ is $\mathcal{O}(N_s^2 N_r + N_r^3)$ and $\mathcal{O}(N_r^2 N_d + N_d^3)$, respectively, the overall computational complexity of solving the problem (11) can be estimated as $\mathcal{O}(N_s^2 N_r + N_r^3 + N_r^2 N_d + N_d^3 + k_1(c_0 + c_1 c_2)N_2)$ using the primal decomposition based algorithm, and $\mathcal{O}(N_s^2 N_r + N_r^3 + N_r^2 N_d + N_d^3 + k_2 c_3 N_2)$ with the upper bound based algorithm, where k_1 and k_2 are the number of bisection searches needed to obtain the optimal α. The computational complexity of the algorithm in [2] is given by $\mathcal{O}(N_s^2 N_r + N_r^3 + N_r^2 N_d + N_d^3 + k_3 c_4 N_2)$, where k_3 and c_4 are the number iterations required for optimizing α and $(\mathbf{x}, \mathbf{y})$, respectively. Thus, the proposed algorithms have a similar computational complexity order to the approach in [2].

D. Peak Power Constraint

With only the energy constraints (7) and (10) in the problem (11), the transmission power at the source and relay nodes may increase to a large value when α approaches 0 or 1. To impose a constraint on the peak transmission power at the source node during the energy transfer phase, we introduce $\lambda_b \leq P_{m,s}$, where $P_{m,s}$ is the peak power at the source node. Based on (16),

this is equivalent to

$$\sum_{i=1}^{N_2} y_i \le \frac{2\alpha P_{m,s}}{1-\alpha} - P_0, \quad \alpha > \alpha_0 \tag{52}$$

where $\alpha_0 = \frac{P_0}{2P_{m,s}+P_0}$. Considering constraints on the peak transmission power at the source and relay nodes during the information transfer phase, we have

$$\sum_{i=1}^{N_2} x_i \le P_{m,s} \tag{53}$$

$$\sum_{i=1}^{N_2} \lambda_{f,i}(\lambda_{h,i}\lambda_{2,i}+1) = \eta\tilde{\lambda}_{h,1}\sum_{i=1}^{N_2} y_i \le P_{m,r} \tag{54}$$

where $P_{m,r}$ is the peak power at the relay node. Both $P_{m,s}$ and $P_{m,r}$ depend on factors such as the system hardware and electromagnetic interference requirements. By adding constraints (52)–(54) into the problem (18), we have the following power allocation problem with peak power constraints

$$\min_{\alpha,\mathbf{x},\mathbf{y}} \ \frac{1-\alpha}{2}\sum_{i=1}^{N_2}\log\frac{1+a_i x_i+b_i y_i}{(1+a_i x_i)(1+b_i y_i)} \tag{55a}$$

$$\text{s.t.} \ \sum_{i=1}^{N_2} x_i + \sum_{i=1}^{N_2} y_i \le P_s\frac{1+\alpha}{1-\alpha} - P_0 \tag{55b}$$

$$\sum_{i=1}^{N_2} x_i \le P_{m,s} \tag{55c}$$

$$\sum_{i=1}^{N_2} y_i \le \min\left(\frac{2\alpha P_{m,s}}{1-\alpha} - P_0, \frac{P_{m,r}}{\tilde{\eta\lambda}_{h,1}}\right) \tag{55d}$$

$$\alpha_0 < \alpha < 1, \ x_i \ge 0, \ y_i \ge 0, \ i = 1,\ldots,N_2. \tag{55e}$$

For a given α, the problem (55) can be viewed as a power allocation problem in a two-hop MIMO relay system with both sum power constraint across the source and the relay nodes (55b) and individual power constraints at the source node (55c) and the relay node (55d). This makes the problem (55) even harder to solve than the problem (18). Interestingly, by studying which constraints in (55) are tight, the problem (55) can be divided into the sum power constraint case which can be solved by Algorithm 1, and the individual power constraint case which can be solved by existing works such as [2].

An exact analysis on the value of (55a) is very difficult even without the constraints (55c) and (55d), as it is mentioned before, the analysis of the value of (18a) subjecting to (18b) is hard. With the individual power constraints (55c) and (55d), the feasible region of the problem (55) is smaller compared with that of the problem (18). Therefore, the optimum of (55a) subjecting to (55b)–(55e) might be larger than the optimum of (18a) under (18b)–(18c). The following lemma summarizes the impact of (55c) and (55d) on the value of (55a).

Lemma 2: The constraint (55c) affects the value of (55a) for $\alpha \in [\alpha_x, 1)$, and (55d) changes the value of (55a) for $\alpha \in (\alpha_0, \alpha_y]$ and $\alpha \in [\alpha_z, 1)$, where $\alpha_0 < \alpha_x, \alpha_y, \alpha_z < 1$ are threshold parameters. In particular, as $P_{m,s}$ and $P_{m,r}$ decrease, α_x and α_z decrease, while α_y increases.

Proof: Firstly, we compare the two constraints (55b) and (55c). As $P_s\frac{1+\alpha}{1-\alpha} - P_0$ increases with α, the feasible region specified by (55b) expands when α increases. Thus, there exists an $\alpha_x \in (\alpha_0, 1)$ such that for $\alpha_0 < \alpha < \alpha_x$, (55c) is less strict than (55b), while (55c) becomes active for $\alpha_x \le \alpha < 1$. Obviously, as the feasible region defined by (55c) shrinks when $P_{m,s}$ decreases, this indicates that (55c) becomes active for a smaller α_x when $P_{m,s}$ decreases.

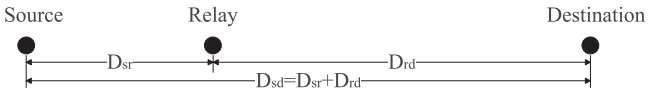

Fig. 5. Source, relay, and destination placement.

Secondly, we compare the two constraints (55b) and (55d). Let us rewrite (55d) as

$$\sum_{i=1}^{N_2} y_i \le \frac{2\alpha P_{m,s}}{1-\alpha} - P_0, \quad \alpha \le \alpha_1 \tag{56}$$

$$\sum_{i=1}^{N_2} y_i \le \frac{P_{m,r}}{\eta\tilde{\lambda}_{h,1}}, \quad \alpha_1 \le \alpha < 1 \tag{57}$$

where $\alpha_1 = \frac{\varpi}{2P_{m,s}+\varpi}$ and $\varpi = \frac{P_{m,r}}{\eta\tilde{\lambda}_{h,1}} + P_0$. As $\frac{2\alpha P_{m,s}}{1-\alpha} - P_0$ increases with α, there exists an $\alpha_y \in (\alpha_0, \alpha_1]$ such that for $\alpha_0 < \alpha \le \alpha_y$, constraint (56) is stricter than (55b). As α increases, there also exists an $\alpha_z \in [\alpha_1, 1)$ such that (57) is stricter than (55b) for $\alpha_z \le \alpha < 1$. Moreover, the feasible region specified by (55d) shrinks when $P_{m,r}$ and/or $P_{m,s}$ decrease. This implies that (55d) is active for a larger α_y and a smaller α_z when $P_{m,s}$ and $P_{m,r}$ decrease, respectively. ■

The three 'Peak Power Constraints' curves in Fig. 3 show the optimum of (55a) (i.e., $F(\alpha)$) subjecting to (55b)–(55e) where $P_{m,s} = P_{m,r} = \kappa P_s$, with $\kappa = 1$, $\kappa = 2$, and $\kappa = 10$, respectively. It can be seen that the peak power constraints (55c) and (55d) indeed change the value of $F(\alpha)$ particularly for smaller κ where the feasible region defined by (55c) and (55d) is small. Interestingly, for $\kappa = 10$, (55c) and (55d) only increase the value of $F(\alpha)$ when α approaches 0 or 1, and they do not affect $F(\alpha)$ in the middle range of α. When $\kappa = 2$, $F(\alpha)$ is affected by (55c) and (55d) for a wider range of α. For $\kappa = 1$, the peak power constraints greatly change $F(\alpha)$ for the whole range of $0 < \alpha < 1$. These observations verify Lemma 2. Moreover, in the example of Fig. 3, the minimum of $F(\alpha)$ remains unchanged for $\kappa = 2$ and $\kappa = 10$, but increases under $\kappa = 1$. Interestingly, for all three κ, $F(\alpha)$ is still a unimodal function of α as shown in Fig. 3.

IV. Simulations

In this section, we study the performance of two proposed algorithms through numerical simulations. We consider a scenario where the three nodes are located in a line as shown in Fig. 5. Without specifically mentioned, the distance between the source node and the destination node is $D_{sd} = 20$ meters, and the source-relay and relay-destination distances are $D_{sr} = 10d$ meters and $D_{rd} = 10(2-d)$ meters, respectively,[4] where the value of $0 < d < 2$ is normalized over a distance of 10 meters. The reason of such normalization is to make it easy to identify whether the relay node is located closer to the source node ($0 < d < 1$) or closer to the destination node ($1 < d < 2$). Similar to [27], [28], [37], the channel matrices are modeled as $\mathbf{H} = D_{sr}^{-\zeta/2}\bar{\mathbf{H}}$

[4]This is among the typical distance of RF-based wireless power transfer reported in [36].

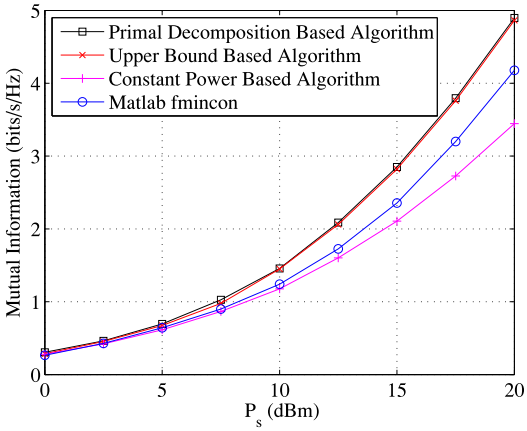

Fig. 6. Example 1: MI versus P_s with energy constraint only, $N = 5$, $d = 1$.

and $\mathbf{G} = D_{rd}^{-\zeta/2}\bar{\mathbf{G}}$, where $D_{sr}^{-\zeta}$ and $D_{rd}^{-\zeta}$ are the large-scale path loss and $\bar{\mathbf{H}}$ and $\bar{\mathbf{G}}$ denote the small-scale Rayleigh fading. Here ζ is the path loss exponent. Considering the suburban propagation environment, we choose $\zeta = 3$ [37]. $\bar{\mathbf{H}}$ and $\bar{\mathbf{G}}$ have independent and identically distributed (i.i.d.) complex Gaussian entries with zero-mean and variances of $1/N_s$ and $1/N_r$, respectively. In the simulations, we choose $0.1 < d < 1.9$ such that $D_{sr} > 1$ and $D_{rd} > 1$. The noise power at the relay and the destination nodes is fixed as $\sigma_r^2 = \sigma_d^2 = -50$ dBm. For all simulation examples, we fix $N_s = N_r = N_d = N_2 = N$. The per-antenna static power consumption at the relay node is set to $P_c = 1\ \mu$W. We compare the performance of the proposed primal decomposition based algorithm (Algorithms 1, 2, and 3) and the upper bound based approach (Algorithms 1 and 4) with the algorithm in [2], which is denoted as the constant power based algorithm as the constraints (8) are employed in [2]. All the numerical simulation results are averaged over 1000 independent channel realizations.

A. Example 1: MI Versus the Nominal Source Node Power

In the first example, we set $d = 1$. The MI of three algorithms versus the nominal power P_s is shown in Fig. 6 with $N = 5$ for $\eta = 0.8$. As a benchmark, the system MI by using the Matlab fmincon tool to solve the problem (18) is also shown in Fig. 6. We observe from Fig. 6 that the two proposed algorithms perform better than the Matlab fmincon algorithm and the constant power based algorithm in [2] throughout the whole range of P_s. Moreover, the MI gap between both proposed algorithms and that of the fmincon algorithm and the constant power based algorithm increases with P_s. In fact, at $P_s = 20$ dBm, the proposed algorithms achieve a 40% increase of the MI of the constant power based algorithm.

Fig. 7 shows the MI of three algorithms versus the nominal power P_s with $N = 3$ for $\eta = 0.8$ and $\eta = 0.5$. It can be seen from Fig. 7 that the system achieves a lower rate at $\eta = 0.5$ compared with that at $\eta = 0.8$. In the following, we choose $\eta = 0.8$ in the simulations. Interestingly, we can observe from Figs. 6 and 7 that the performance of the two proposed algorithms is almost the same. The reason is that for the upper bound based algorithm, the bound error $1/((1 + a_i x_i)(1 + b_i y_i))$ is small as $a_i x_i$ and $b_i y_i$ are much larger than 1 under practical wireless powered relay communication scenarios. Therefore, both proposed algorithms converge to the same optimal performance.

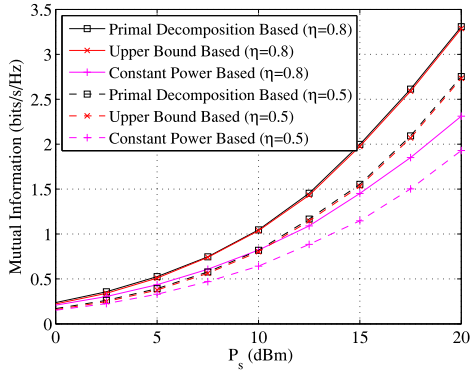

Fig. 7. Example 1: MI versus P_s with energy constraint only, $N = 3$, $d = 1$.

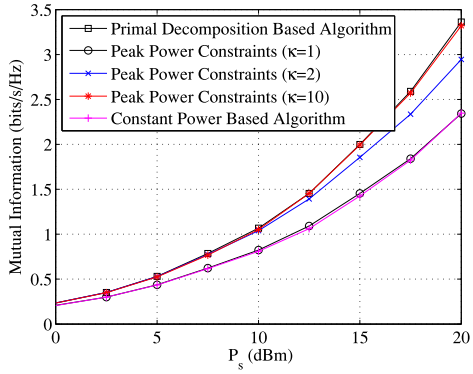

Fig. 8. Example 1: MI versus P_s with peak power constraints, $N = 3$, $d = 1$.

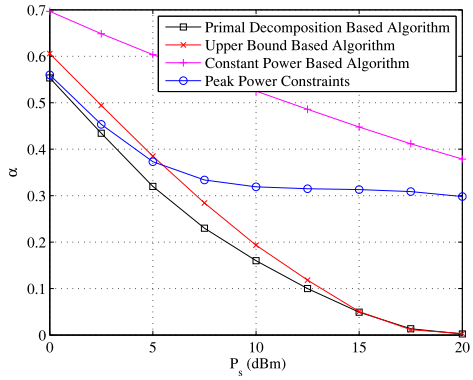

Fig. 9. Example 2: Optimal α versus P_s, $N = 3$, $d = 1$.

By comparing Fig. 6 with Fig. 7, we can see that the achievable rate increases with the number of antennas.

Fig. 8 shows the system MI versus P_s with $N = 3$ considering the peak power constraints. We set $P_{m,r} = P_{m,s} = \kappa P_s$ with $\kappa = 1$, $\kappa = 2$, and $\kappa = 10$. It can be seen that the achievable MI increases with κ. Interestingly, the system MI with $\kappa = 1$ is similar to that of the constant power based algorithm. This indicates that the proposed framework includes the algorithm in [2] as a special case.

B. Example 2: Time Switching Factor Versus the Nominal Source Node Power

In the second example, we set $N = 3$ and $d = 1$. The time switching factors α calculated as optimal by three algorithms versus the nominal power P_s are shown in Fig. 9. It can be

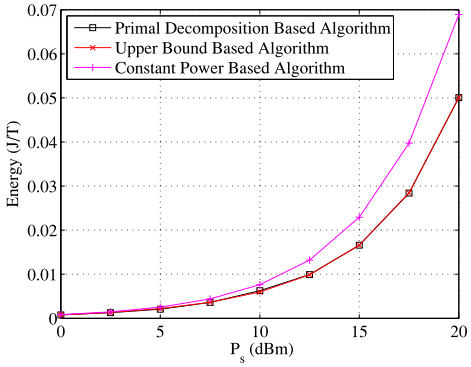

Fig. 10. Example 3: Total system energy consumption versus P_s, $N = 3$, $d = 1$.

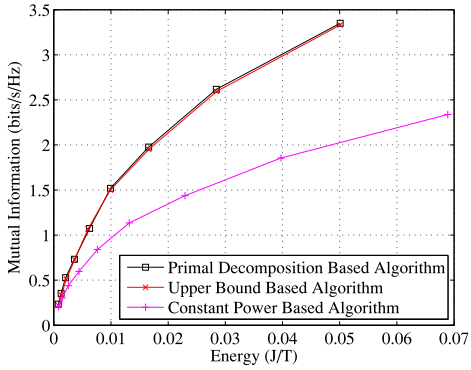

Fig. 11. Example 3: MI versus total system energy consumption, $N = 3$, $d = 1$.

seen from Fig. 9 that for all three algorithms, the optimal α monotonically decreases as the nominal power P_s increases. The reason is that as P_s increases, a smaller α is sufficient for the relay node to harvest the energy required for forwarding the information signals.

Moreover, we observe from Fig. 9 that the optimal α of the two proposed algorithms are very close to each other, and the optimal α for the system with peak power constraints where $P_{m,r} = P_{m,s} = 2P_s$ is similar to that of the constant power based algorithm. Interestingly, the variation of α in the two proposed algorithms throughout the range of P_s is larger than that of the fixed power algorithm. In fact, for both proposed algorithms, the optimal α becomes very small when P_s is at 20dBm. The reason is that when P_s is large enough, λ_b (the power level at the source node at the first interval) obtained by the proposed algorithms increases. Thus, even though α is small, the energy $\alpha\eta\tilde{\lambda}_{h,1}\lambda_b$ harvested by the relay node is sufficient for forwarding the signal to the destination node. Therefore, for both proposed algorithms, more time is allocated for information transmission so that a higher data rate can be achieved at large P_s.

C. Example 3: MI and Energy Consumption Trade-Off Comparison

We observe from Fig. 9 that the optimal α obtained by the two proposed algorithms is smaller than that in [2]. Since the power-carrying signals are transmitted at the same nominal power P_s from the source node to the relay node, we can expect that the energy consumed by the proposed algorithms is less than that by [2]. This is confirmed by Fig. 10 where the total system energy consumption of three algorithms $\frac{1+\alpha}{2}P_s$ (measured in Joule per time T) is plotted versus P_s for $N = 3$ and $d = 1$. It can also be seen from Fig. 10 that the two proposed algorithms consume a similar amount of energy.

Interestingly, from Figs. 6 and 10, we can see that for a given P_s, the two proposed algorithms achieve a higher MI while consuming less energy. Hence, the proposed algorithms have a better rate-energy trade-off than the constant power based algorithm. This fact is further illustrated by Fig. 11 where we plot the MI versus energy of three algorithms for $N = 3$ and $d = 1$. It can be clearly seen from Fig. 11 that the energy efficiency of the proposed algorithms is much higher than that of the constant power based algorithm. In fact, with the energy of 0.05 J/T, the MI achieved by the proposed algorithm is 70% more than that of the constant power based algorithm.

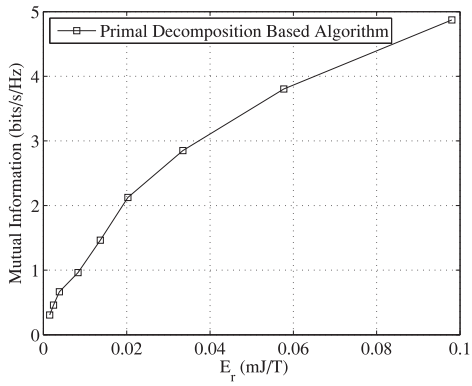

Fig. 12. Example 3: MI versus energy harvested at the relay node, $N = 5$, $d = 1$.

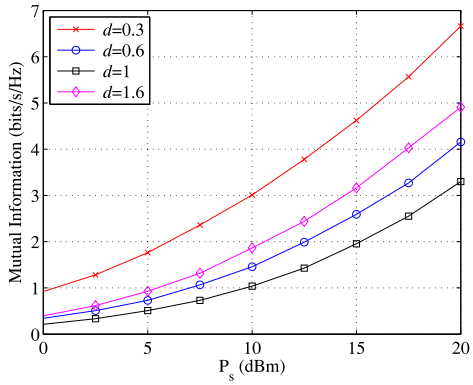

Fig. 13. Example 4: MI of the upper bound based algorithm versus P_s at various d, $N = 3$.

Fig. 12 shows the system MI versus the energy harvested at the relay node E_r in (2) for $N = 5$ and $d = 1$. It can be clearly seen that the system achievable data rate increases with E_r. Thus, $\eta_2 E_r$ increases with the amount of information processing and it is sensible to adopt $\eta_2 E_r$ as the dynamic part of the circuit energy consumption in Section II.

D. Example 4: Achievable MI at Various Distances

In the last example, we study the impact of source-relay distance on the achievable MI. First we set $N = 3$ and study the achievable MI at various d. Fig. 13 shows the MI of the upper bound based algorithm versus P_s at various d. The performance

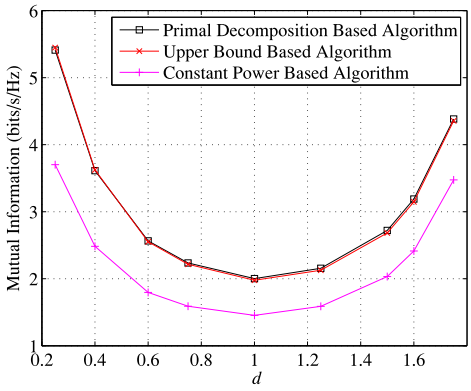

Fig. 14. Example 4: MI versus d, $P_s = 15$ dBm, $N = 3$.

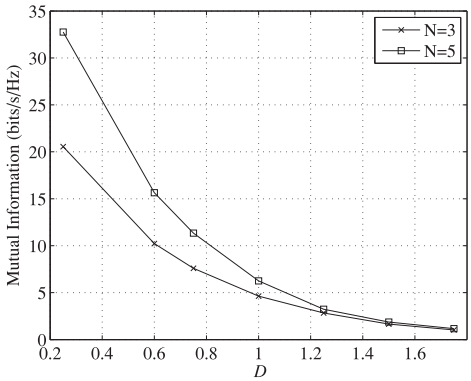

Fig. 15. Example 4: MI versus D, $P_s = 15$ dBm.

of the primal decomposition based algorithm is not shown in Fig. 13 as it has a similar MI as the upper bound based algorithm. Fig. 14 shows the MI of all three algorithms versus d with $N = 3$ and $P_s = 15$ dBm. It can be seen from Figs. 13 and 14 that for the three algorithms tested, the achievable MI first decreases when d increases and then increases again with the growth of d. The reason is that when the relay node is closer to the source node, it can harvest more energy and consequently, the MI is higher. When the relay node is very close to the destination node, although the amount of harvested energy is smaller, the shorter relay-destination distance and thus a better second-hop channel improves the system MI. Moreover, it can be observed from Fig. 14 that the proposed algorithms have an MI gain of 0.5–1.5 bits/s/Hz over the constant power based algorithm over the whole range of d.

Finally, we investigate the impact of the source-destination distance. Here we set the source-relay and relay-destination distances as $D_{sr} = 5D$ meters and $D_{rd} = 10D$ meters, respectively. Thus, the source-destination distance is $D_{sd} = 15D$ meters. It can be seen from Fig. 15 that compared with a three-antenna system, having five antennas can improve the source-destination distance.

V. Conclusion

We have investigated the transceiver optimization for TS-based wireless information and energy transfer in two-hop non-regenerative MIMO relay systems. Compared with the fixed power constraint at the source node used in existing works, a more general energy constraint at the source node has been proposed. The optimal structure of the source and relay precoding matrices has been derived and a two-loop method has been developed to solve the transceiver optimization problem. Numerical simulations show that both proposed algorithms yield much higher system MI and better rate-energy tradeoff than the constant power based method. We have found that the value of the optimal time switching factor decreases as the nominal power of the source node increases, and the system MI increases with the energy harvested at the relay node. Interestingly, we have observed that with a fixed source-destination distance, the achievable MI is higher as the relay node gets closer to the source node or the destination node, and other factors such as the accessibility should be considered when determine the position of the relay node.

Appendix A
Proof of Theorem 1

The following result from [38] is needed to prove Theorem 1.

Lemma 3 [38, H.1.g]: For two $n \times n$ positive semidefinite matrices $\mathbf{U}$ and $\mathbf{V}$, there is $\mathrm{tr}(\mathbf{UV}) = \sum_{i=1}^{n} \lambda_i(\mathbf{UV}) \leq \sum_{i=1}^{n} \lambda_i(\mathbf{U})\lambda_i(\mathbf{V})$, where $\lambda_i(\mathbf{A})$ denotes the ith eigenvalue of matrix $\mathbf{A}$, $\lambda_i(\mathbf{U})$ and $\lambda_i(\mathbf{V})$, $i = 1, \ldots, n$, are sorted in the same order.

Now we start to prove Theorem 1. First we prove the optimal structure of $\mathbf{B}_1$. It can be seen from the problem (11) that $\mathbf{B}_1$ does not appear explicitly in the objective function (11a), and it affects (11a) through changing the feasible region of the problem specified by the constraints (11b) and (11c). Therefore, in order to maximize the feasible region, for *any* $\mathrm{tr}(\mathbf{B}_1\mathbf{B}_1^H)$, we should maximize $\mathrm{tr}(\mathbf{H}\mathbf{B}_1\mathbf{B}_1^H\mathbf{H}^H)$, which can be written as the following optimization problem

$$\max_{\mathbf{B}_1} \ \mathrm{tr}(\mathbf{H}\mathbf{B}_1\mathbf{B}_1^H\mathbf{H}^H) \tag{58a}$$

$$\text{s.t.} \ \ \mathrm{tr}(\mathbf{B}_1\mathbf{B}_1^H) = \lambda_b \tag{58b}$$

where λ_b is a positive scalar.

Let us introduce the eigenvalue decomposition of $\mathbf{B}_1\mathbf{B}_1^H = \mathbf{U}_1\mathbf{\Lambda}_1\mathbf{U}_1^H$, where the diagonal elements of $\mathbf{\Lambda}_1$ are sorted in decreasing order (same as $\mathbf{\Lambda}_h$ in (12)). From Lemma 3, we have $\mathrm{tr}(\mathbf{H}\mathbf{B}_1\mathbf{B}_1^H\mathbf{H}^H) \leq \sum_{i=1}^{N_s} \tilde{\lambda}_{h,i}\lambda_{1,i}$, where $\tilde{\lambda}_{h,i}$ and $\lambda_{1,i}$ denote the ith diagonal element of $\mathbf{\Lambda}_h$ and $\mathbf{\Lambda}_1$, respectively, and the equality is achieved if and only if $\mathbf{U}_1 = \mathbf{V}_h\mathbf{\Phi}$. Here $\mathbf{\Phi}$ is an $N_s \times N_s$ diagonal matrix with unit norm diagonal elements, i.e., $|\phi_{i,i}| = 1$, $i = 1, \ldots, N_s$. Without affecting the values of (58a) and (58b), we choose $\mathbf{\Phi} = \mathbf{I}_{N_s}$, and thus $\mathbf{U}_1 = \mathbf{V}_h$. Hence, the problem (58) becomes

$$\max_{\boldsymbol{\lambda}_1} \ \sum_{i=1}^{N_s} \tilde{\lambda}_{h,i}\lambda_{1,i} \qquad \text{s.t.} \ \ \sum_{i=1}^{N_s} \lambda_{1,i} = \lambda_b \tag{59}$$

where $\boldsymbol{\lambda}_1 = [\lambda_{1,1}, \ldots, \lambda_{1,N_s}]^T$. Obviously, the solution of the problem (59) is $\lambda_{1,1} = \lambda_b$ and $\lambda_{1,i} = 0$, $i = 2, \ldots, N_s$. Thus, we have $\mathbf{B}_1\mathbf{B}_1^H = \lambda_b\mathbf{v}_{h,1}\mathbf{v}_{h,1}^H$. Therefore, we prove

$$\mathbf{B}_1^* = \lambda_b^{\frac{1}{2}}\mathbf{v}_{h,1}. \tag{60}$$

By substituting (60) back into the problem (11), we have the problem of

$$\max_{0<\alpha<1,\lambda_b,\mathbf{B}_2,\mathbf{F}} \ \mathrm{MI}(\alpha,\mathbf{B}_2,\mathbf{F}) \tag{61a}$$

$$\text{s.t.} \quad \mathrm{tr}(\mathbf{B}_2\mathbf{B}_2^H) \le \frac{2}{1-\alpha}\left(\frac{1+\alpha}{2}P_s - \alpha\lambda_b\right) \tag{61b}$$

$$\mathrm{tr}(\mathbf{F}(\mathbf{H}\mathbf{B}_2\mathbf{B}_2^H\mathbf{H}^H + \sigma_r^2\mathbf{I}_{N_r})\mathbf{F}^H) \le \frac{2\alpha\eta}{1-\alpha}\lambda_b\tilde{\lambda}_{h,1} - N_rP_c. \tag{61c}$$

It can be seen that for *any* given α and λ_b, the problem (61) is in the same form as the problem (13)–(15) in [13]. Therefore, $\mathbf{B}_2^*$ and $\mathbf{F}^*$ in (13) are proven based on Theorem 1 in [13]. ■

Appendix B
Proof of Lemma 1

For the simplicity of notations, in the proof we write $\mu(p_i,a_i,b_i)$ as $\mu(p_i)$ when we prove the unimodality of μ with respect to p_i, and write $\mu(p_i,a_i,b_i)$ as $\mu(a_i)$ and $\mu(b_i)$, respectively, when we prove μ monotonically increases with a_i and b_i. From (29) and (30), we have the first-order derivatives of $\mu_1(p_i)$ and $\mu_2(p_i)$ as

$$\mu_1'(p_i) = \frac{2a_ib_ip_i + a_i + b_i}{2\sqrt{(a_ip_i+1)(b_ip_i+1)}} \tag{62}$$

$$\mu_2'(p_i) = \frac{a_ib_i(a_i-b_i)^2}{2(a_i\sqrt{b_ip_i+1} - b_i\sqrt{a_ip_i+1})^2\sqrt{(a_ip_i+1)(b_ip_i+1)}}. \tag{63}$$

Using (62) and (63), we have

$$\mu'(p_i) = \frac{\mu_2'(p_i)\mu_1(p_i) - \mu_1'(p_i)\mu_2(p_i)}{\mu_1^2(p_i)} = \frac{a_ib_i(\mu_3(p_i)-\mu_4(p_i))}{2(a_i\sqrt{b_ip_i+1}-b_i\sqrt{a_ip_i+1})^2\sqrt{(a_ip_i+1)^3(b_ip_i+1)^3}} \tag{64}$$

where

$$\mu_3(p_i) = (2a_ib_ip_i + a_i + b_i)^2 \tag{65}$$

$$\mu_4(p_i) = 2a_ib_i\sqrt{(a_ip_i+1)(b_ip_i+1)}(a_ip_i + b_ip_i + 2). \tag{66}$$

In the following, we show that $\mu'(p_i) = 0$ has only one root for $p_i \ge 0$.

From (64)–(66), we know that the root of $\mu'(p_i) = 0$ is equal to the root of the following equation

$$J_1(p_i) = \mu_3^2(p_i) - \mu_4^2(p_i) = -4a_i^2b_i^2(a_i-b_i)^2J(p_i) = 0 \tag{67}$$

where

$$J(p_i) = a_ib_ip_i^4 + (a_i+b_i)p_i^3 - p_i^2 - \left(\frac{2}{a_i}+\frac{2}{b_i}\right)p_i - \frac{a_i^2+b_i^2+6a_ib_i}{4a_i^2b_i^2}. \tag{68}$$

From (68) we have

$$J'(p_i) = 4a_ib_ip_i^3 + 3(a_i+b_i)p_i^2 - 2p_i - \left(\frac{2}{a_i}+\frac{2}{b_i}\right) \tag{69}$$

$$J''(p_i) = 12a_ib_ip_i^2 + 6(a_i+b_i)p_i - 2 \tag{70}$$

where $J'(p_i)$ and $J''(p_i)$ are the first-order and second-order derivatives of $J(p_i)$, respectively. It can be clearly seen from (68)–(70) that $J(0) < 0$, $J'(0) < 0$, $J''(p_i) < 0$ for $0 \le p_i < p_{i,0}$ and $J''(p_i) > 0$ for $p_i > p_{i,0}$, where $p_{i,0}$ is the positive root of $J''(p_i) = 0$ give by

$$p_{i,0} = \frac{-3(a_i+b_i) + \sqrt{9a_i^2 + 42a_ib_i + 9b_i^2}}{12a_ib_i}.$$

Therefore, $J(p_i)$ can cross zero only once for $p_i \ge 0$. Thus, we know from (67) that $\mu'(p_i) = 0$ has only one root for $p_i \ge 0$. As a result, $\mu(p_i)$ is a unimodal function of p_i.

Now we start to prove that $\mu(a_i)$ is a monotonically increasing function of a_i. We have from (29), (30), and (34) that

$$\mu(a_i) = \bar{\mu}_1(a_i)\bar{\mu}_2(a_i) \tag{71}$$

where

$$\bar{\mu}_1(a_i) = \sqrt{\frac{a_ib_i}{(a_ip_i+1)(b_ip_i+1)}} \tag{72}$$

$$\bar{\mu}_2(a_i) = \frac{\sqrt{a_ib_i}(\sqrt{a_ip_i+1} - \sqrt{b_ip_i+1})}{a_i\sqrt{b_ip_i+1} - b_i\sqrt{a_ip_i+1}}. \tag{73}$$

Obviously, $\bar{\mu}_1(a_i)$ monotonically increases with a_i. After several steps, we find that the first-order derivative of $\bar{\mu}_2(a_i)$ with respect to a_i can be written as

$$\bar{\mu}_2'(a_i) = \frac{(a_i-b_i)(\sqrt{a_ip_i+1}-\sqrt{b_ip_i+1})}{2\sqrt{a_i^3b_i(a_ip_i+1)}\left(\sqrt{\frac{a_i}{b_i}(b_ip_i+1)} - \sqrt{\frac{b_i}{a_i}(a_ip_i+1)}\right)^2} \tag{74}$$

where we can see $\bar{\mu}_2'(a_i) \ge 0$. From (71) we have

$$\mu'(a_i) = \bar{\mu}_1(a_i)\bar{\mu}_2'(a_i) + \bar{\mu}_1'(a_i)\bar{\mu}_2(a_i). \tag{75}$$

Since $\bar{\mu}_1(a_i) \ge 0$, $\bar{\mu}_2(a_i) \ge 0$, $\bar{\mu}_1'(a_i) \ge 0$, and $\bar{\mu}_2'(a_i) \ge 0$, we know from (75) that $\mu'(a_i) \ge 0$, which indicates that $\mu(a_i)$ is a monotonically increasing function of a_i. As (72) and (73) have a symmetric structure with respect to a_i and b_i, we can prove that $\mu(b_i)$ is a monotonically increasing function of b_i similar to (71)–(75). ■

Acknowledgment

The authors would like to thank the editor and anonymous reviewers for their valuable comments and suggestions that helped improve the quality of the paper.

References

[1] Z. Ding *et al.*, "Applications of smart antenna technologies in simultaneous wireless information and power transfer," *IEEE Commun. Mag.*, vol. 53, no. 4, pp. 86–93, Apr. 2015.

[2] K. Xiong, P. Fan, C. Zhang, and K. B. Letaief, "Wireless information and energy transfer for two-hop nonregenerative MIMO-OFDM relay networks," *IEEE J. Sel. Areas Commun.*, vol. 26, no. 8, pp. 1397–1407, Aug. 2015.

[3] L. R. Varshney, "Transporting information and energy simultaneously," in *Proc. IEEE Int. Symp. Inf. Theory*, Toronto, ON, Canada, Jul. 2008, pp. 1612–1616.

[4] X. Zhou, R. Zhang, and C. K. Ho, "Wireless information and power transfer: Architecture design and rate-energy tradeoff," *IEEE Trans. Commun.*, vol. 61, no. 11, pp. 4754–4767, Nov. 2013.

[5] R. Zhang and C. K. Ho, "MIMO broadcasting for simultaneous wireless information and power transfer," *IEEE Trans. Wireless Commun.*, vol. 12, no. 5, pp. 1989–2001, May 2013.

[6] B. Clerckx and E. Bayguzina, "Waveform design for wireless power transfer," *IEEE Trans. Signal Process.*, vol. 64, no. 23, pp. 6313–6328, Dec. 2016.
[7] Y. Zeng, B. Clerckx, and R. Zhang, "Communications and signals design for wireless power transmission," *IEEE Trans. Commun.*, vol. 65, no. 5, pp. 2264–2290, May 2017.
[8] B. Li, C. Z. Wu, H. H. Dam, A. Cantoni, and K. L. Teo, "A parallel low complexity zero-forcing beamformer design for multiuser MIMO systems via a regularized dual decomposition method," *IEEE Trans. Signal Process.*, vol. 63, no. 16, pp. 4179–4190, Aug. 2015.
[9] B. Li, H. H. Dam, A. Cantoni, and K. L. Teo, "A first-order optimal zero-forcing beamformer design for multiuser MIMO systems via a regularized dual accelerated gradient method," *IEEE Commun. Lett.*, vol. 19, no. 2, pp. 195–198, Feb. 2015.
[10] B. Li, Y. Rong, J. Sun, and K. L. Teo, "A distributionally robust linear receiver design for multiaccess space-time block coded MIMO systems," *IEEE Trans. Wireless Commun.*, vol. 16, no. 1, pp. 464–474, Jan. 2017.
[11] Q. Shi, L. Liu, W. Xu, and R. Zhang, "Joint transmit beamforming and receieve power splitting for MISO SWIPT," *IEEE Trans. Wireless Commun.*, vol. 13, no. 6, pp. 3269–3280, Jun. 2014.
[12] X. Tang and Y. Hua, "Optimal design of nonregenerative MIMO wireless relays," *IEEE Trans. Wireless Commun.*, vol. 6, no. 4, pp. 1398–1407, Apr. 2007.
[13] Y. Rong, X. Tang, and Y. Hua, "A unified framework for optimizing linear nonregenerative multicarrier MIMO relay communication systems," *IEEE Trans. Signal Process.*, vol. 57, no. 12, pp. 4837–4851, Dec. 2009.
[14] Y. Rong, "Joint source and relay optimization for two-way linear nonregenerative MIMO relay communications," *IEEE Trans. Signal Process.*, vol. 60, no. 2, pp. 6533–6546, Dec. 2012.
[15] A. A. Nasir, X. Zhou, S. Durrani, and R. A. Kennedy, "Relaying protocols for wireless energy harvesting and information processing," *IEEE Trans. Wireless Commun.*, vol. 12, no. 7, pp. 3622–3636, Jul. 2013.
[16] Z. Ding, S. M. Perlaza, I. Esnaola, and H. V. Poor, "Power allocation strategies in energy harvesting wireless cooperative networks," *IEEE Trans. Wireless Commun.*, vol. 13, no. 2, pp. 846–860, Feb. 2014.
[17] Z. Ding, I. Esnaola, B. Sharif, and H. V. Poor, "Wireless information and power transfer in cooperative networks with spatially random relays," *IEEE Trans. Wireless Commun.*, vol. 13, no. 6, pp. 4400–4453, Aug. 2014.
[18] H. Chen, Y. Li, Y. Jiang, Y. Ma, and B. Vucetic, "Distributed power splitting for SWIPT in relay interference channels using game theory," *IEEE Trans. Wireless Commun.*, vol. 14, no. 1, pp. 410–420, Jan. 2015.
[19] Y. Liu and X. Wang, "Information and energy cooperation in OFDM relaying: Protocols and optimization," *IEEE Trans. Veh. Technol.*, vol. 65, no. 7, pp. 5088–5098, Jul. 2016.
[20] C. Zhong, H. A. Suraweera, G. Zheng, I. Krikidis, and Z. Zhang, "Wireless information and power transfer with full duplex relaying," *IEEE Trans. Commun.*, vol. 62, no. 10, pp. 3447–3461, Oct. 2014.
[21] Z. Wen, X. Liu, N. C. Beaulieu, R. Wang, and S. Wang, "Joint source and relay beamforming design for full-duplex MIMO AF relay SWIPT systems," *IEEE Commun. Lett.*, vol. 20, no. 2, pp. 320–323, Feb. 2016.
[22] H. Liu, K. J. Kim, K. S. Kwak, and H. V. Poor, "Power splitting-based SWIPT with decode-and-forward full-duplex relaying," *IEEE Trans. Wireless Commun.*, vol. 15, no. 11, pp. 7561–7577, Nov. 2016.
[23] B. K. Chalise, Y. D. Zhang, and M. G. Amin, "Energy harvesting in an OSTBC based nonregenerative MIMO relay system," in *Proc. IEEE Int. Conf. Acoust., Speech, Signal Process.*, Mar. 2012, pp. 3201–3204.
[24] B. K. Chalise, W. K. Ma, Y. D. Zhang, H. Suraweera, and M. G. Amin, "Optimum performance boundaries of OSTBC based AF-MIMO relay system with energy harvesting receiver," *IEEE Trans. Signal Process.*, vol. 61, no. 17, pp. 4199–4213, Sep. 2013.
[25] Z. Chu, M. Johnston, and S. Le Goff, "SWIPT for wireless cooperative networks," *Electron. Lett.*, vol. 51, no. 6, pp. 536–538, Mar. 2015.
[26] G. Amarasuriya, E. G. Larsson, and H. V. Poor, "Wireless information and power transfer in multiway massive MIMO relay networks," *IEEE Trans. Wireless Commun.*, vol. 15, no. 6, pp. 3837–3855, Jun. 2016.
[27] Y. Huang and B. Clerckx, "Joint wireless information and power transfer for an autonomous multiple-antenna relay system," *IEEE Commun. Lett.*, vol. 19, no. 7, pp. 1113–1116, Jul. 2015.
[28] Y. Huang and B. Clerckx, "Relaying strategies for wireless-powered MIMO relay networks," *IEEE Trans. Commun.*, vol. 15, no. 9, pp. 6033–6047, Sep. 2016.
[29] B. Li and Y. Rong, "AF MIMO relay systems with wireless powered relay node and direct link," *IEEE Trans. Commun.*, vol. 66, no. 4, pp. 1508–1519, Apr. 2018.
[30] A. Antoniou and W.-S. Lu, *Practical Optimization: Algorithms and Engineering Applications*. New York, NY, USA: Springer, 2007.
[31] D. P. Palomar and M. Chiang, "A tutorial on decomposition methods for network utility maximization," *IEEE J. Sel. Areas Commun.*, vol. 24, no. 8, pp. 1439–1451, Aug. 2006.
[32] K. Xiong, P. Fan, Y. Lu, and K. B. Letaief, "Energy efficiency with proportional rate fairness in multirelay OFDM networks," *IEEE J. Sel. Areas Commun.*, vol. 34, no. 5, pp. 1431–1447, May 2016.
[33] Y. Li, Y. Tian, and C. Yang, "Energy-efficient coordinated beamforming under minimal data rate constraint of each user," *IEEE Trans. Veh. Technol.*, vol. 64, no. 6, pp. 2387–2397, Jun. 2015.
[34] S. Boyd and L. Vandenberghe, *Convex Optimization*. Cambridge, U.K.: Cambridge Univ. Press, 2004.
[35] R. G. Eustáquio, E. W. Karas, and A. Ribeiro, "Constraint qualification for nonlinear programming," Federal Univ. Paraná, Curitiba, Brazil, Tech. Rep., May 2008.
[36] X. Lu, D. Niyato, P. Wang, D. I. Kim, and Z. Han, "Wireless charger networking for mobile devices: Fundamentals, standards, and applications," *IEEE Wireless Commun.*, vol. 22, no. 2, pp. 126–135, Apr. 2015.
[37] C. Song, J. Park, B. Clerckx, I. Lee, and K.-J. Lee, "Generalized precoder designs based on weighted MMSE criterion for energy harvesting constrained MIMO and multiuser MIMO channels," *IEEE Trans. Wireless Commun.*, vol. 15, no. 12, pp. 7941–7954, Dec. 2016.
[38] A. W. Marshall, I. Olkin, and B. C. Arnold, *Inequalities: Theory of Majorization and Its Applications*. New York, NY, USA: Springer, 2011.

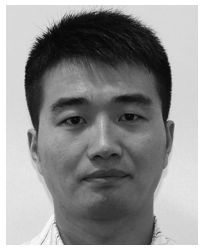

Bin Li (M'18–SM'18) received the Bachelor's degree in automation and the Master's degree in control science and engineering from the Harbin Institute of Technology, Harbin, China, in 2005 and 2008, respectively, and the Ph.D. degree in mathematics and statistics from Curtin University, Perth, WA, Australia, in 2011. From 2012–2014, he was a Research Associate with the School of Electrical, Electronic and Computer Engineering, the University of Western Australia, Perth, WA, Australia. From 2014–2017, he was a Research Fellow with the Department of Mathematics and Statistics, Curtin University. He is currently a Research Professor with the School of Electrical Engineering and Information, Sichuan University, Chengdu, China. His research interests include signal processing, wireless communications, optimization, and optimal control.

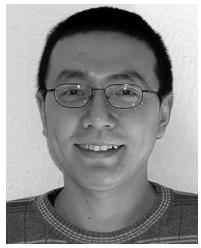

Yue Rong (S'03–M'06–SM'11) received the Ph.D. degree (summa cum laude) in electrical engineering from the Darmstadt University of Technology, Darmstadt, Germany, in 2005.

He was a Post-Doctoral Researcher with the Department of Electrical Engineering, University of California, Riverside, Riverside, CA, USA from February 2006 to November 2007. Since December 2007, he has been with the Department of Electrical and Computer Engineering, Curtin University, Bentley, Bentley, WA, Australia, where he is currently a Professor. He has authored or coauthored more than 150 journal and conference papers. His research interests include signal processing for communications, wireless communications, underwater acoustic communications, applications of linear algebra and optimization methods, and statistical and array signal processing.

Dr. Rong was a recipient of the Best Paper Award at the 2011 International Conference on Wireless Communications and Signal Processing, the Best Paper Award at the 2010 Asia-Pacific Conference on Communications, and the Young Researcher of the Year Award of the Faculty of Science and Engineering at Curtin University in 2010. He is an Associate Editor for the IEEE TRANSACTIONS ON SIGNAL PROCESSING. He was an Editor for the IEEE WIRELESS COMMUNICATIONS LETTERS from 2012 to 2014, a Guest Editor for the IEEE JOURNAL ON SELECTED AREAS IN COMMUNICATIONS special issue on theories and methods for advanced wireless relays, and a TPC Member for the IEEE ICC, the IEEE GlobalSIP, WCSP, IWCMC, EUSIPCO, and ChinaCom.